An Analytical Spectroscopic Method for the Reliable Determination of Binding Constants and Fluorescent Rare Earth Element Detection

A Thesis

Presented in Partial Fulfillment of the Requirements for the

Degree of Master of Science

with a

Major in Chemical Engineering

in the

College of Graduate Studies

University of Idaho

by

Samuel R. Wolfe

Major Professor: James Moberly, Ph.D.

Committee Members: Kristopher Waynant, Ph.D.; Mark Roll, Ph.D.

Department Chair: D. Eric Aston, Ph.D.

August 2018

Authorization to Submit Thesis

The thesis of Samuel R. Wolfe, submitted for the degree of Master of Science with a Major in Chemical Engineering and titled "An Analytical Spectroscopic Method for the Reliable Determination of Binding Constants and Fluorescent Rare Earth Element Detection" has been reviewed in final form. Permission, as indicated by the signatures and dates below, is now granted to submit final copies to the College of Graduate Studies for approval.

Major Professor: _____ Date: _____
James Moberly, Ph.D.

Committee Members: _____ Date: _____
Kristopher Waynant, Ph.D.

_____ Date: _____
Mark Roll, Ph.D.

Department
Administrator: _____ Date: _____
Eric Aston, Ph.D.

Abstract

Metal residues are found widely distributed in products and waste streams and recovery and detection of these materials is desirable. This thesis investigated the detection of rare earths in different matrices and determination of binding constants for characterizing N,N-diethylphenylarylazothioformamide (ATF) ligand. Low level fluorometric dectection of rare earths was investigated for Nd, Sm, and Eu in place of UV/Vis using the arsenazo-III ligand. Unfortunately, fluorometric detection was comparable to UV/Vis levels of detection and quantification. Metal-binding ligands, such as ATF, are a possible solution for purification of materials and recovery of valuable metals. However, binding of ATF to metals must be characterized to engineer it‘s affinity to metals. Ligand characterization showed cooperative binding between the redox active ATF ligand and Cu(I) salts. Characteristic UV/Vis and ^{1}H NMR models were coupled for more reliable binding constant determination. In general, coupling two measurement methods increases the reliability of determined parameters.

Acknowledgements

I would like to acknowledge all the staff and professors in the Chemical Engineering department at the University of Idaho for their support in completing my classes and research in the short amount of time that I did, it would not have been possible without out their help. I would also like to include the researchers in the Dr. Waynant's lab for the help in experiments and data collection for my research, as well as psychological support. I want to acknowledge my graduate committee for the advice and help in completing my thesis on quick deadlines. I also want to thank Dr. Kris Waynant for the many meetings of moral support and overall motivations to complete my thesis, he is by far one of my favorite professors at the University of Idaho. Finally, I would like to wholly thank and acknowledge my major professor Dr. James Moberly for taking on the large risk of having me as his graduate student and without his advice, guidance, and support throughout my graduate career I would not have my degree or the career opportunities I now have. Thank you, Dr. Moberly.

Dedication

I would like to dedicate this thesis and the motivation for earning both my B.S. and M.S. entirely to my mother Elizabeth Wolfe for all the love and support that she has provided throughout my academic career and life, without her sacrifice I would not be the man I am today.

Table of Contents

List of Figures

List of Tables

List of Equations

Chapter 1: Introduction

Metal species are widely used as catalysts in the production of pharmaceuticals, consumer care products, polymers, fuels, and carbon materials.[1–7] Consequently, due to high production throughput or inadequate cleaning methods, metal residues are commonly found to exist at undesirable quantities in the final products. Due to potential toxicities, lack of therapeutic benefit, possible side reactions, and loss of valuable catalyst the priority for a remedial process is high for industry.[8,9] Impurity removal in chemical synthesis, nanomaterial design, and polymer industries includes concerns of weight, purity, and altered material properties.[10–12] In the example of double walled carbon nanotubes, specific synthesis methods leave iron nano particles within nanotubes that contributes considerably to the overall weight of the product and dramtically alters the electrochemical properties of the nanotubes.[10,11,13] Making metal residue removal methods that do not harm the consumer or the product while retaining valuable catalyst extremely attractive.

Trace metal detection from waste streams containing lost catalyst is also important for metal recovery. For example the supply of rare earth elements (REE) is situated in an economically insecure state due to 90% of global demand satisfied by a near monopolized source and global demand overwhelming availability.[14–16] Necessitating the development of supply chain diversification, one method of focus for research is REE screening and recovery from waste streams or natural water sources.[17–19]

In both cases metal-binding ligands may provide a solution to the removal of metallic residues from products and the subsequent recovery of REEs from waste water streams or natural water sources.[20–24] Coordination chemistry describes a ligand as an ion or a molecule that coordinates with a central metal atom, or another ionic species.[25] The resulting coordination of the metal and ligand is referred to as the metal-ligand complex, which arises due to the intermolecular interactions between the metal and ligand species.[25,26]

1.1 Host:Guest Models

Host:guest interactions in supramolecular chemistry are a central area of study in many chemical disciplines such as organic, inorganic, and organometallic reactions specifically for an analytical determination of association/disassociation constants. Host:guest complexation

chemistry was pioneered by supramolecular chemists Donald and Jane Cram in the 1970s for illustrating active sites in enzymatic catalysis for organic reactions.[27,28] Many examples of host ligands binding with guest metals are observed in biological systems, a representative example is of protoporphyrin IX binding with guest iron to form heme in the production of hemoglobin.[29] Synthetic host ligands coordinating with metal ions have undergone much investigation, the earliest involved host cyclic polyethers binding with various metal salts.[30] Host:guest models provide a method for describing the noncovalent coordination of molecules, which is essential in supramolecular chemistry for demystifying the intricacies of molecular recognition and binding. **Figure 1.1** shows a simple example of 1:1 host:guest complexation from complementary binding sites due to favorable stereoelectronic relationships of charge and shape.[27] **Figure 1.1** is represented mathematically as an equilibrium equation, shown in **Eq. (1.1)**.

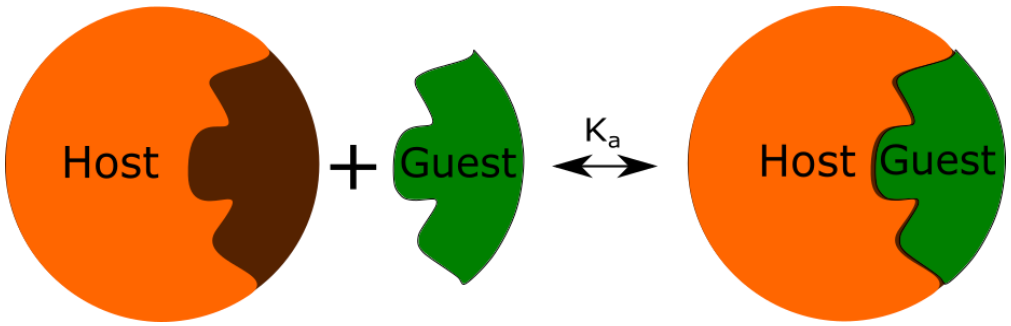

Figure 1.1: Schematic for simple 1:1 binding of host to guest

$$H + G \overset{K_a}{\leftrightarrow} HG \tag{1.1}$$

$$K_a = \frac{[HG]}{[H][G]} \tag{1.2}$$

$$\Delta G^o = -RTln\,(K_a) \tag{1.3}$$

Binding equilibriums and the inherent strength of association between host and guest are defined by binding constants, traditionally chemist describe binding with the association constant (K_a), whereas biochemist tend to describe binding using the dissociation constant (K_d) which is an inverse of K_a.[25] Association constants are defined in terms of concentration as a ratio of formed host:guest complex (*HG*) over the free host (*H*) multiplied by free guest

(*G*), **Eq. (1.2)**. The association constants quantitatively represent host:guest complexation behavior and are interpreted thermodynamically as a direct correlation of the intrinsic stabilities, expressed as change in Gibbs free energy, shown in **Eq. (1.3)** as an indicator of the energy needed to convert host and guest to a host:guest complex.[25]

Biding constants are a desirable measurement for understanding the energy requirements and strength of host:guest complexation. In the case of 1:1 binding of host to guest, the model is relatively straightforward and comprehensive with the only assumptions being that one of species involved in binding is "silent" and the observed physical change is correlated to the concentration of *HG*, *H*, and *G*.[31,32] As and example **Eq. (1.4)** represents a measurement with some observable physical change (*Y*) in the system (i.e. chemical shift for NMR or absorbance change for UV-Vis) defined by the contribution of *H*, *G*, and *HG* concentrations, multiplied by their specific physical change factors. *H* and *G* can be defined in terms of initial concentrations and *HG* concentration through material balances seen in **Eq. (1.5)** and **(1.6)**. Host and guest physical change factors may also be determined by pure species dilution experiments where observed physical change only depends linearly on host or guest concentrations, in this example it is assumed that the guest is silent ($Y_G = 0$), simplifying the final equation. Substituting **Eq. (1.3)** into **(1.5)** and **(1.6)**, then substituting derived equations for *H* and *HG* into **Eq. (1.4)** gives **Eq. (1.7)** as a generic host:guest model for 1:1 binding, leaving only the host:guest complex physical change factor and association constant as unknown parameters.[31–33]

$$Y_{obs} = Y_H[H] + Y_G[G] + Y_{HG}[HG] \tag{1.4}$$

$$[H]_0 = [H] + [HG] \tag{1.5}$$

$$[G]_0 = [G] + [HG] \tag{1.6}$$

$$Y_{obs} = \frac{[H]_0(2Y_H - Y_{HG}(1 + K_{a1}([H]_0 - [G]_0) - \sqrt{(K_{a1}([H]_0 - [G]_0) + 1)^2 + 4[G]_0K_{a1}}}{\sqrt{(K_{a1}([H]_0 - [G]_0) + 1)^2 + 4[G]_0K_{a1}} - K_{a1}([H]_0 - [G]_0) + 1} \tag{1.7}$$

When 1:2 or 2:1 binding is suspected, similar steps in derivation are taken with the addition of another binding step represented in **Eq. (1.8)**, however considerations into whether there is cooperativity between the two binding sites are necessary, as this will cultivate different host:guest models. Cooperativity between binding sites indicates a stepwise binding where the first binding site to be occupied by a guest will influence the binding of the second guest.[25,31] Conversely, if the binding sites are non-cooperative then both sites are identical and the steps in complexation are independent events. Any additive effects in the physical change factors, where the factors double from *HG* when forming the second binding complex HG_2 or H_2G (i.e. $Y_{H_2G} = 2Y_{HG}$), will result in a separate host:guest binding model. Accounting for these different binding conditions brings about several model variations for describing 1:2 or 2:1 host:guest binding, including the "full" cooperative model, the non-cooperative model, the additive model, and the statistical model which is a combination of non-cooperative and additive assumptions.[31,34]

Cooperative binding

In 1:2 or 2:1 host guest binding interactions between host and guest becomes a stepwise process that depends on the sequence of which binding site is occupied first and whether the occupancy of one binding site alters the subsequent binding of the remaining site. In the example of two guests binding to one host (2:1), if the initial binding of the first guest to an unoccupied host alters the affinity for a second guest to occupy the remaining site, the binding mechanism is considered cooperative, illustrated by **Figure 1.2**.[25,31] The change in affinity may increase or a decrease the second association constant (K_{a2}) for the final complex, **Eq. (1.9),** depending on the intermolecular forces between bound hosts and guests.[25,31]

$$HG + G \overset{K_{a2}}{\longleftrightarrow} H_2G \tag{1.8}$$

$$K_{a2} = \frac{[H_2G]}{[HG][G]} \tag{1.9}$$

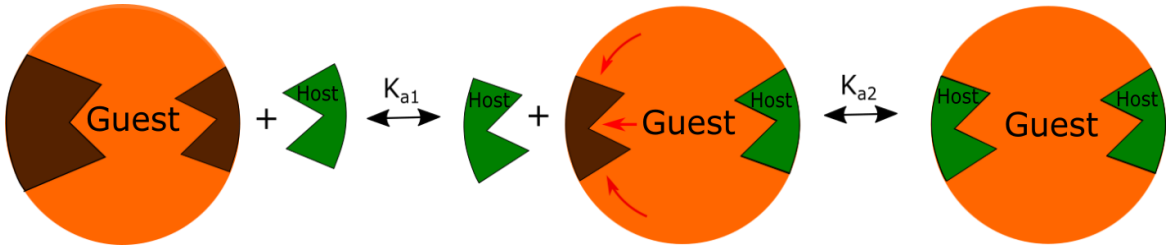

Figure 1.2: Schematic of cooperative binding for a 2:1 host:guest system.

Cooperativity would indicate that the two binding sites do not experience mutually independent binding events. Consequently, K_{a1} for the initial binding will influence the value of K_{a2}, due to the change in affinity, but it is not possible to relate the K_{a1} to K_{a2} because the change is too complex to correlate.[31] Cooperative binding is assumed when developing the "full" model of host:guest binding where the K_{a1} and K_{a2} are two independent constants for the generic 2:1 model shown in **Eq. (1.10)**. The generic model is in terms of *H* from the material balances shown in **Eq. (1.11)** and **(1.12)** where a cubic equation, **Eq. (1.13)** must be solved to determine the logical root for *H* to use in **Eq. (1.10)**.[31,33]

$$Y_{obs} = Y_H[H] + \frac{[G]_0[Y_{HG}K_1[H] + 2(Y_{H_2G}K_{a1}K_{a2}[H]^2)]}{1 + K_{a1}[H] + K_{a1}K_{a2}[H]^2} \tag{1.10}$$

$$[H]_0 = [H] + [HG] + 2[H_2G] \tag{1.11}$$

$$[G]_0 = [G] + [HG] + [H_2G] \tag{1.12}$$

$$[H]^3(A) + [H]^2(B) + [H](C) - [H]_0 = 0 \tag{1.13}$$

$$With:\ A = K_{a1}K_{a2}$$

$$B = K_{a1}(2K_{a2}[G]_0 - K_{a2}[H]_0 + 1)$$

$$C = K_{a1}([G]_0 - [H]_0) + 1$$

However, if it is assumed that the binding sites do experience mutually independent binding events, due to truly identical sites, then the binding may be considered non-cooperative.

Non-cooperative Binding

In the case of non-cooperative binding both binding sites are unaffected by the stepwise binding that occurs before hand.[31,34] As a result, there are two open binding sites initially, site A and site B, each with identical binding potentials but two possible pathways for complexation where either site A or site B is occupied initially, followed by the remaining site to form the 2:1 complex. **Figure 1.3** represents the pathways for non-cooperative binding, both pathways have their respective microscopic association constants represented by K_{1A} and K_{2A} for the case where site A is initially bound, or K_{1B} and K_{2B} for the case where site B is

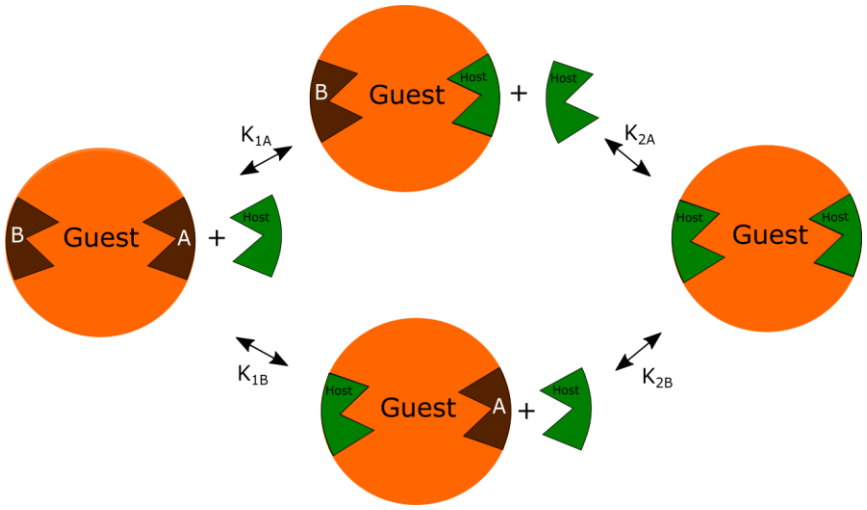

Figure 1.3: Schematic for non-cooperative binding in a 2:1 host:guest system.

$$[HG] = [HG_{1A}] + [HG_{1B}] \tag{1.14}$$

$$K_{a1} = K_{1A} + K_{1B} \tag{1.15}$$

$$K_{a2} = \frac{K_{2A}K_{2B}}{K_{2A} + K_{2B}} \tag{1.16}$$

$$K_{a1} = 4K_{a2} \tag{1.17}$$

bound initially. Since both binding sites are identical in their binding potential and physical change then the microscopic association constants for each site are equal and can be defined in terms of the macroscopic association constants K_{a1} and $K_{a2.}$ From **Eq. (1.3)** the concentration of *HG* may be defined as a sum of the two initial pathway steps represented by **Eq. (1.10)** allowing K_{a1} to be defined by **Eq. (1.11)**. Similarly, using **Eq. (1.4)**, K_{a2} may defined as **Eq. (1.12)**. Finally, with the assumption that each pathway has identical binding characteristic each pathway's microscopic association constants may be defined as overall microscopic constants for each path K_{1M} and K_{2M}, where $K_{1A} = K_{1B} = K_{1M}$ and $K_{2A} = K_{2B} = K_{2M}$.[31] Since it is assumed that there is no influence on the empty binding site what so ever, then $K_{1M} = K_{2M}$, this relationship allows the macroscopic association constants K_{a1} and K_{a2} to be correlated mathematically, shown in **Eq. (1.13),** as a factor of four.[31]

1.2 Spectroscopic Analysis

Routine methods for quantitative analysis of host:guest binding phenomena include fluorescent, UV-visible, nuclear magnetic resonance spectroscopies, quartz crystal microbalance, and isothermal titration calorimetry studies.[25,35] Each technique seeks to determine the same disassociation/association constants for describing the intermolecular interactions of coordinating molecules.[25] The most common method for quantifying complexation is through spectroscopic titration studies by measuring the physical change during additions of guest species into host solutions, traditionally through either proton NMR (^{1}H NMR), UV-Vis, or fluorescence.[25,31,36] As discussed physicals changes of the resulting complex, relative to the individual host and guest species, correlates to association constant (K_a) through each measurements characteristic equation.

Proton NMR

In the case of ^{1}H NMR the complex often causes a shift in proton orientation changing the specific chemical resonance that can be observed over multiple titrations of guest species into host solution and provide valuable insights into the possible structure of the resulting complex and binding stoichiometry.[25] However, the timescale for ^{1}H NMR measurements is slow compared to the exchange rates of complexation resulting in a combinational spectrum that is an average of the host:guest complex and host or guest, depending on which is NMR

invisible. This means that the chemical shift of the pure host and guest is additional unknown that must be solved for, adding to the error associated with the determined association constants in the host:guest system.[25] As a result most NMR titration models are defined as a change in chemical shift from the baseline of pure host or guest.

Photochemical processes, such as absorbance and fluorescence, operate on a rapid observation regime by takin place on timescales of picoseconds (ps) for absorbance, and nanoseconds (ns) or less for fluorescence, resulting in individual signals from each species present in the host:guest system, as opposed to a combinational spectrum from NMR.[25] Individual observable species in the spectra highlights why UV-Vis and fluorescence spectroscopy is advantageous when conducting titration studies.

UV-Vis Spectroscopy

A molecule may absorb a photon when exposed to light with a suitable amount of energy, promoting the molecule to an excited electronic state. Photon absorption is most commonly explained using the visible spectrum of light, approximately 400-700nm, where substances reflect some portions or wavelengths of light while absorbing others and this can be observed visually by color. Colorless samples may still absorb light in regions outside the visible light range including ultraviolet and infrared. Absorption efficiency is expressed experimentally as the molar extinction coefficient, ϵ, in Beer's law.[25] Beer's law is the linear relationship between concentration and the optical density or absorbance of a sample, the ratio of incident radiation and transmitted radiation.[25] It is important to note that absorbance is a logarithmic quantity that limits accuracy as absorbance values exceed a value of 2, indicating that 99% of the incident light has been absorbed.[25] Because the efficiency of absorption is not constant at every wavelength the extinction coefficient, and as a result absorbance, is function of wavelength. A plot of absorbance versus wavelengths is called an absorbance spectrum, this shows the relative change in electronic states over various wavelengths. In the case of UV-Vis spectroscopy the spectrum is referred to as UV/vis spectra.[25]

Spectra analysis is important in the case of analyzing multicomponent solutions or mixtures because monitoring the change in the UV/vis spectra as additions of guest are added into the host solution gives insight into regions in the spectra that are related to the complexation events. The complexation of host and guest becomes a third absorbing species

in the sample resulting which result in either an additive effect on the overall observed absorbance peak or the resulting host:guest complex may absorb at wavelengths in which the pure host/guest might not, giving a distinct absorbance peak separate from host and guest. The latter case is much more beneficial for experimental determination of host:guest binding but is not always a result of complexation.

Fluorescence

Conversely to absorption, where a photon is absorbed promoting the molecule to an excited electronic state, the molecule may revert to the ground electronic state through the concomitant emission of a photon. The emission of photon is referred to as fluorescence and, like absorption, varies as a function of wavelength. Plots of fluorescence intensity as a function of wavelength are called fluorescence spectra or emission spectra.[25] Because fluorescence first requires the excitation of a molecule into a higher energy state prior to measuring the emission of a photon, the resulting spectra is a combination of absorption and fluorescence spectrum, commonly referred to as excitation and emission spectra.

The advantages of fluorescence spectroscopy are that two absorption signals at the same wavelength would be more difficult to distinguish in a UV/vis spectrum but could easily be identified in fluorescence spectra, given that the emission of the two molecules occurs at separate wavelengths. Additionally, fluorescence is a zero-background technique because the sample is irradiated at one wavelength and detected at a separate wavelength there should be no background irradiation reaching the detector, making fluorescence a very sensitive measurement method.[25] However not all molecules participate in fluorescence and simply dissipated excess energy from irradiation as heat into the system through internal conversion. As a solution there are commercially available dyes, or chelating ligands, that do fluoresce individually, and upon binding with ionic compounds such as calcium, or rare earth elements, show an increase in fluorescence intensity. Coupled with the sensitivity of fluorescence measurements, these ligands allow for the detection of trace level concentrations of cationic species such as rare earth elements.

1.3 Quantitative Analysis

Second to carefully designed experiments and measurements, proper data analysis is essential to understanding host:guest chemistry. Traditional supramolecular chemistry quantitative analysis involved linear regression methods that involved linearizing governing equations such that they can be plotted to determine K_a and other physical parameters from observed slope and intercepts.[25] Examples of these methods include the popular Benesi-Hildebrand plot, or Lineweaver-Burke plot for enzyme kinetics, the Scott or Hanes-Woolf transformations, the Scatchard plot, and the continuous variation method or Job plot.[37–43] Although convenient and computationally simple, these methods have become antiquated with the development of software capable to handle intense computational modelling that allows for a more accurate prediction by eliminating possibly unfavorable assumptions or shortcuts.[31,34] Employing software, such as MATLAB, capable of non-linear regression analysis and exact solutions to quadratic or cubic equations that can arise from host:guest modelling of higher order coordinated complexation eliminates the need for using linear transformation methods.[31]

As discussed 1:1 host guest binding is quantitatively simple for determining association constants, but when 1:2 or 2:1 binding is suspected the binding is much more complex with respect to reliably determining an association constant. Resulting from a secondary binding phenomenon each adjustable parameter doubles leading to a system with four fitting parameters, including association constants for the first and second binding events (K_{a1} & K_{a2}) and physical change variables for each host guest complex that occurs. From a mathematical standpoint a system with four fitting parameters and only three independent variables will inevitably lead to overfitting of the data and a deceptive result for best fit parameters. The measured parameters and unknown/fitted parameters for of each model is presented in **Table 1.1**.

Table 1.1: Measure and fitted parameters for 1:1 and 2:1 host:guest binding models.

1:1 Host:guest parameters		2:1 Host:guest parameters	
Measured	**Unknown/Fitted**	**Measured**	**Unknown/Fitted**
$[H]_0$	Y_{HG}	[H]	Y_{HG}
$[G]_0$	K_{a1}	$[G]_0$	K_{a1}
Y_H		Y_H	Y_{H_2G}
			K_{a2}

Due to overfitting conditions vastly different parameter values with magnitudes of difference could still be considered "best fit" parameters through observably equal goodness-of-fit to experimental measurements.[44] Host:guest models coupled with non linear fitting methods provides a useful tool for an accurate determination of association constants that forgoes antiquated linear regression methods.

The coalition of detection, host:guest modelling, and quantitave analysis of metal-binding ligands provides a tool for screening ligands for the use as metal scavangers as well as trace metal detetectors. Tools for metal detection and metal recovery will aid in reducing the wide distribution of trace metals lost in waste streams or final products. In the case of metal scavanging investigations into redox active ligands, such as the arylazothioformamide class of ligands, may give increased functionailty for metal binding.[21,22] Redox ligands also show flexibility in the binding coordination by participating in both 1:1 and 2:1 binding with Cu(I) species, this variable binding makes the ligand a advantageous system for exploring reliable methods for the determination of association constants. In the case of detection methods, a poplular fluorophore ligand known to bind to cations called arsenazo-III may provide lower level detection along with more reliable determinatoin of trace rare earth elements in various aqeuous systems.

Chapter 2: ATF Binding with Copper**(I)** Species

Copper catalyzed synthesis continues to grow and consequently due to deleterious effects of Cu(I) contamination, including cytotoxicity, DNA damage, and oxidative lesions, removal of residual copper species from heterogeneous materials may become more important.[45,46] Nielsen, Bechgaard, and Krebs have effectively employed redox-active arylazothioformamide (ATF) ligands to remove residual Pd and Cu nanoparticles from conjugated polymers by precipitating the polymer and ligand solution, then separating the insoluble polymer from the soluble ligand-metal complex.[20–22]

The azothioformamide (ATF) ligand class can participate in three possible redox states (neutral, singly reduced, and doubly reduced), shown in **Figure 2.1**. Predicting the oxidation states of complexes containing redox-active ligands can be a difficult task. [47–51] Previous works by Bechgaard and Krebs through cyclic voltammetry experiments and crystallographic analysis have suggested a two to one binding to form a coordinated complex with copper(I) tetrakis(acetonitrile) tetrafluoroborate ($CuBF_4$) without agreement on the oxidation states of the copper center and bound ligands.[52] Bechgaard predicted two oxidation states included [(Cu^{I}(ATF^{*-})(ATF)], with a singly reduced ligand coupled with one innocent (neutral) ligand, and alternatively [(Cu^{II}(ATF^{*-})(ATF^{*-})], where the copper center has become divalent and binds with two singly reduced ligands. These discontinuities along with the multiple valence states of copper outlines the difficulties in predicting the oxidation states and coordination of metal-ligand complexes. Recently, oxidation states for metal-ligand coordination complexes have become less ambiguous with advances in computational modeling and X-ray crystallographic analyses.[53] Structural evidence using these methods shows that copper centers stay in the Cu(I) oxidation state while participating in 2:1 binding with Cu(I)BF_4 and Cu(I)PF_6, contrasted by an alternate 1:1 binding with Cu(I)Br, Cu(I)I, and Cu(I)Cl.[53]

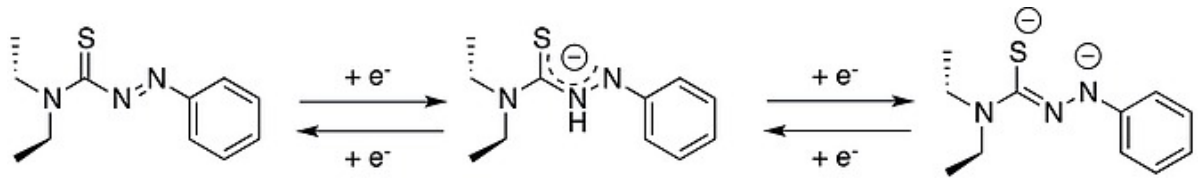

Figure 2.1: Neutral (left), singly reduced (middle), and doubly reduces (right) ATF ligand

In the case of Cu(II) interactions the redox nature of ATF may further complicate the coordination of ATF host with Cu guest, even in the event of predicted 1:1 binding, through the addition of multistep equilibrium constants that arise, possibly through a reduction of the Cu(II) to Cu(I) prior to binding. The redox behavior of the ATF ligand allows for participation in multiple binding coordination that depend on the valence states of the guest metal species. It is this flexibility in binding that highlights the worth of ATF ligands as a system to investigate different binding interactions for establishing a reliable determination of association constant values.

2.1 Methods

Reagents: Copper (I) iodide (98%) was purchased from AK Scientific, Copper (I) bromide (98%) tetrakis(acetonitrile) copper (I) tetrafluoroborate (now refer to as CuBF4), tetrakis(acetonitrile) copper (I) hexafluorophosphate (CuPF6) were purchased from Sigma Aldrich, CH3CN (Fisher Scientific), CD3CN (Cambridge Isotopes).

N,N-Diethylphenylazothioformamide synthesis:

The synthesis of the N,N-diethylphenylazothioformamide ligand was conducted according to previously publishes methods.[53]

2.1.1 UV-Vis Titrations

Dilution curves

Pure host and guest extinction coefficients (ϵ_H, ϵ_G) were defined through a linear fit of absorbance change over several concentrations. Unfortunately, there is no practical method for measuring the amount of HG created in the system and therefore ϵ_{HG} cannot be determined analytically. Dilution curves were produced by preparing a stock solution of ATF dissolved in acetonitrile at 0.1125mM. Starting with pure species at this stock concentration, the absorbance spectra was measured using a ThermoFisher GENESYS 60S UV-Vis Spectrophotometer. Dilutions were then performed in succession by adding 40 L aliquots of acetonitrile to 1.2mL of stock ATF using a Thermofisher Finnpipette F1 Pipette and measuring the absorbance spectra after each aliquot addition, this was repeated 50 times until a final volume of 3.2mL was achieved. The same dilution procedure described for ATF was performed for both CuBr, CuI, $CuBF_4$, and $CuPF_6$ dissolved in acetonitrile.

ATF-Cu Titrations

UV-Vis spectroscopic titration studies of ATF and copper began by adding fractional molar equivalents of copper to ATF solutions. Starting with the same stock concentration of ATF as the dilution procedure, 0.1125 mM, stock solutions of CuBr, CuI, $CuPF_6$, and $CuBF_4$ in acetonitrile were made at a concentration such that a volume of 10 μL would hold a molar equivalent of 0.1 compared to the stock ATF solution, this resulted in a stock concentration of 1.35 mM for each copper species. Following an absorption spectra measurement of pure species ATF with an initial volume of 1.2 mL, 0.1 equivalents of individual copper solutions were added in aliquots of 10 μL prior to measuring the absorbance spectra after each aliquot addition. This procedure was repeated 30 times until a total of 3 molar equivalents of copper species to ATF was achieved. These titration studies resulted in the ATF-Cu absorbance spectra seen in **Figure 2.2**, where shifts can be observed from the pure ATF absorbance spectra to the final ATF-Cu complex absorbance spectra for each coordinated complex.

2.1.2 NMR Titrations

ATF-Cu Halide Titrations:

5.0 mg of ATF (0.03016 mmoles) was added to 14 NMR tubes. Cu(I) halides were added to each tube in variable amounts to accomplish 0.25 molar equivalent steps ranging from 0.10 equivalents to 3.00 equivalents. The solution volumes were kept constant and Cu(I) halides were added from a stock solution of 0.1293 M (0.1855 mg of Cu(I) Bromide and 0.2462 mg of in case of Cu(I) Iodide) dissolved in 10 mL of CD3CN. All solutions were kept to 0.70 mL to keep ATF concentration constant at 0.00431 M. All tubes were sonicated for 30 minutes at room temperature before NMR experimentation. All NMRs were conducted on a Bruker Avance 300 MHz instrument referenced to CD3CN delta = 1.93 ppm. Each NMR experiment ran for 16 scans.

ATF-Cu Complex Titrations:

5.0 mg of ATF (0.03016 mmoles) was added to an NMR tube for measurement. Cu(I) complexes were added to the tubes as aliquot addition of 0.1 equivalent moles ranging from 1 equivalent to 10.00 equivalents. Cu(I) complex aliquots were added from a 0.0335 M stock solution in 168 μL volumes. All tubes were sonicated for 30 minutes at room temperature

before NMR experimentation. All NMRs were conducted on a Bruker Avance 300 MHz instrument referenced to CD3CN delta = 1.93 ppm. Each NMR experiment ran for 16 scans.

2.1.3 Host:Guest Models

UV/Vis

ATF complexes with Cu(I) salts show distinct absorption spectra with significant differences from pure ATF ligand spectra, **Figure 2.2** shows the shifts in absorbance peaks from 190-1100 nm at 0.1125 mM concentrations. Choosing an appropriate concentration of ATF such that Beer-Lamberts Law ($A = \epsilon bC$) satisfies the conditions that A has a value less than one, seen at 0.1125mM for ATF, however upon complexing with Cu(I) salts the UV ranges (190-400 nm) exceed values of one due to the additive contribution of the Cu(I) salts that also absorb light at these wavelengths. Fortunately, the absorbance phenomena seen between 500-800 nm is not present for either pure Cu(I) salts or pure ATF spectra meaning this broad peak is distinct for our ATF-Cu complexes.

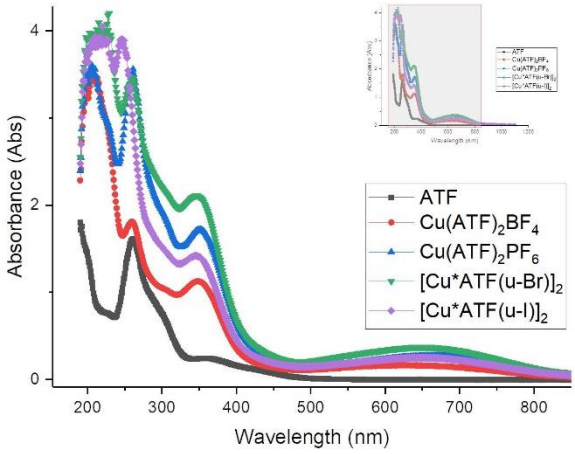

Figure 2.2: Absorption spectra for pure ATF and ATF-Cu Complexes at 0.1125mM

Both 1:1 and 2:1 absorbance models are in terms of concentration of the host ligand (H), the guest copper species (G), the host:guest complexes (HG) and (H_2G), their associated molar attenuation coefficient ϵ_i, and the optical pathlength, b, is constant at a value of 1 cm. The observed absorbance at any wavelength is an additive absorbance value comprised of all the species absorbing at the wavelength of interest. This is described mathematically by the Beer-Lambert law, as the characteristic equation for UV-Vis, in terms of a host:guest system the same Beer-Lambert equation is equivalent to **Eq. (2.1)**, describing the 1:1 binding with copper halides CuI and CuBr, and **Eq. (2.2)**, describing 2:1 binding with copper complexes $CuBF_4$ and $CuPF_6$.

$$A_{obs} = \epsilon_H[H] + \epsilon_G[G] + \epsilon_{HG}[HG] \tag{2.1}$$

$$A_{obs} = \epsilon_H[H] + \epsilon_G[G] + \epsilon_{HG}[HG] + \epsilon_{H_2G}[H_2G] \tag{2.2}$$

Proton NMR

Considerable shifts in proton NMR signals are often observed for a guest binding to a host. This is especially true for cyclophane hosts, such as the ATF ligand, which have aromatic "walls" that can produce large shielding effects. Like the observed absorbance value, the total observed resonance (δ) is an additive quantity that represents the combined effect of the host and host:guest complex to the overall chemical shift. Because the guest Cu species is NMR invisible it is not present in the NMR signal. This is represented mathematically as the characteristic equation for NMR by **Eq. (2.3)** for the 1:1 binding with copper halides and **Eq. (2.4)** for the 2:1 binding with copper complexes in terms of the host mole fraction (X_H), host:guest complex mole fraction (X_{HG}), as well as host and host:guest chemical shifts (δ_i).

$$\delta_{obs} = \delta_H X_H + \delta_{HG} X_{HG} \tag{2.3}$$

$$\delta_{obs} = \delta_H X_H + \delta_{HG} X_{HG} + \delta_{H_2G} X_{H_2G} \tag{2.4}$$

2.1.4 Numerical Analysis:

Full derivations of the 1:1 and 2:1 host:guest models can be found in previous methods defined by literature.[31,32,33] The governing equations are shown in **Eq. (1.1)**, **(1.2)**, **(1.8)**, and **(1.9)** for the associations constants of each binding model. Although the equations that define the disassociation/associations constants are simple in form, the quantitative analysis is not, especially in the case of 2:1 binding due too many unknown parameters with respect to measured variables, as seen in **Table 1.1**, which will lead to an overfitting condition.

1:1 Binding with Cu Halides

Beginning with the 1:1 binding of the host and guest, if it were possible to measure the concentration of the complex, defining the disassociation constant would only require using the mass balance equations, **Eq. (1.10)** and **(1.11)**. The remaining concentrations of the free host and guest could be calculated, and the association constant would be defined. Unfortunately, there is no practical method for measuring the amount of complex formed. Thus, mathematical manipulations to **Eq. (1.2)** and **(1.4)** must be undertaken to derive host:guest model equations in terms of known quantities and "fitting" parameters.

The following model equations describe the observed change in absorbance, **Eq. (2.5)**, and the observed chemical shift, **Eq. (2.6)**, for the case of 1:1 host:guest binding. Because the guest copper species are NMR invisible and non-absorbing in the wavelengths of interest (500-800 nm), their physical change (δ_G and ϵ_G) is treated as zero, eliminating the free guest contribution.

$$A_{obs} = \frac{[H]_0(2\epsilon_H - \epsilon_{HG}(1 + K_{a1}([H]_0 - [G]_0) - \sqrt{(K_{a1}([H]_0 - [G]_0) + 1)^2 + 4[G]_0K_{a1}}}{\sqrt{(K_{a1}([H]_0 - [G]_0) + 1)^2 + 4[G]_0K_{a1}} - K_{a1}([H]_0 - [G]_0) + 1} \quad (2.5)$$

$$\delta_{obs} = \frac{\delta_{HG}\left[\frac{K_{a1}([G]_0 - [H]_0) - 1 + \sqrt{4[G]_0K_{a1} + (K_{a1}([G]_0 - [H]_0) + 1)^2}}{2}\right]}{1 + \left[\frac{K_{a1}([G]_0 - [H]_0) - 1 + \sqrt{4[G]_0K_{a1} + (K_{a1}([G]_0 - [H]_0) + 1)^2}}{2}\right]} \quad (2.6)$$

Both models are in terms of the initial concentrations of host ($[H]_0$) and guest ($[G]_0$), as well as two fitting parameters. The two fitting parameters include a physical change factor inherent to the measurement method and the association constant (K_{a1}). For NMR the physical change is represented by the chemical shift associated with the host:guest complex (δ_{HG}), conversely the molar extinction coefficient of the host:guest complex (ϵ_{HG}) describes the absorbance properties of the complex. Parameters describing the physical change are distinct for each model and therefore considered as "local" fitting parameters, although because K_{a1} is present in both model and the value of K_{a1} is independent of the measurement method it can be treated as a "global" parameter between both models.

Rather than applying traditional methods for simplification and linearization, such as Benesi-Hildebrand plot, that can invalid assumption for the system, such as $[G] \approx [G]_0$ or $Y_{HG} = Y_{obs}$ at the end of the experiment.[31,54,55] The author elected to design optimization methods carried out by the MATLAB® functions reported in the SI. Utilizing the nonlinear multivariable solver function Fmincon, the two model equations can be coupled through the global parameter K_{a1} and solved simultaneously for the disassociations constant as well as physical change variables using the square quadratic programming (SQP) algorithm designed for complex constrained nonlinear optimization.[56] The optimization is essentially "guided" by the reduction of error in the cost function, represented by **Eq. (2.7)**, which is the sum of

squared residuals between the experimentally measured values from both titration methods (UV-Vis and NMR) and the model predicted values from **Eq. (2.8)** and **Eq. (2.9)**.

$$A_{error} = (A_{measured} - A_{model})^2 \quad (2.7)$$

$$\delta_{error} = (\delta_{measured} - \delta_{model})^2 \quad (2.8)$$

$$\text{Cost} = A_{error} + \delta_{error} \quad (2.9)$$

The optimized parameters are determined though a feedback iterative looping method of taking initial guesses for each fitting parameter, provided by the user, then adjusting these values until the cost function reaches a near-zero value set as the function tolerance. Tolerance indicates the goodness-of-fit between experimental values and model predicted values, for this study the model fit must reach a tolerance of 1×10^{-15} in the error value. Additionally, to ensure that the minimum error is a global minimum, rather than a local minimum, the resulting values from a single optimization is taken and a disturbance factor of 50% is multiplied by each fitting parameter, then feedback into the optimization routine as the new initial guess. This process is repeated as many times as the user sees necessary to ensure that the results are the parameters of best fit, this should occur when the answers are consistent despite a range of rational initial guesses and the predicted model graphically fits the experimental measurements values.

2:1 Binding with Cu Complexes

Derivations of the host:models models for 2:1 binding share the same method as the 1:1 derivation with the addition of a second binding phenomenon, represented in the mass balance. Derivations of the cubic equation, shown in **Eq. (1.13)**, and the solution have been outlined in previous literature by using Cardano's method.[31,57] Root determination and screening has been written into the MATLAB function files for the determination of K_{a2}. The resulting host guest models describing the full 2:1 binding of ATF with the Cu complexes $CuBF_4$ and $CuPF_6$ is shown in **Eq. (2.10)** and **(2.11)**. The cost function for the 2:1 binding host:guest models has the same structure as **Eq.(2.9)**, but with the corresponding copper

complex titration measured values and predicted values from the 2:1 host:guest models for UV-Vis and NMR.

$$A_{obs} = \epsilon_H[H] + \frac{[G]_0[\epsilon_{HG}K_{a1}[H] + 2(\epsilon_{H_2G}K_{a1}K_{a2}[H]^2)]}{1 + K_{a1}[H] + K_{a1}K_{a2}[H]^2} \quad (2.10)$$

$$\delta_{obs} = \frac{[G]_0(K_{a1}\delta_{HG}[H] + 2\delta_{H_2G}K_{a1}K_{a2}[H]^2)}{[H]_0(1 + K_{a1}[H] + K_{a1}K_{a2}[H]^2)} \quad (2.11)$$

Upon doing a degree of freedom analysis there are three independent variables and four fitting parameters that inevitably leads to overfitting of the data and meaningless results for the disassociations constant and physical change constants. Meaning that a resulting association constant with magnitude 10^2 would be just as valid as 10^5 when comparing the goodness-of-fit, as an example the comparison between **Figures 2.3-5** show equally good fits but vastly different values for association constants, and **Figure 2.5** a large deviation from reasonable results, this is a huge obstacle in the attempt of defining a disassociation constant. One method that effectively reduces the number of fitting parameters is assuming that if both binding sites of the 2:1 complex are identical and can be described by the non-cooperative binding model where $K_1 = 4K_2$.[31,34] This assumption

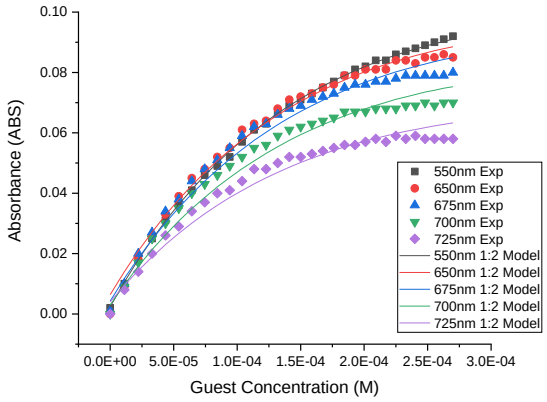

K_{a1} (M^{-1})	K_{a2} (M^{-1})
1,147,124 (±2.52%)	6,266,605 (±2.53%)

Figure2.3: $CuBF_4$ 2:1 Fit with initial guesses K_{a1} = 1,000 M^{-1}, K_{a2} = 5,000 M^{-1}, ϵ_{HG} = 1,000 M^{-1}, ϵ_{H2G} = 1,000 M^{-1}

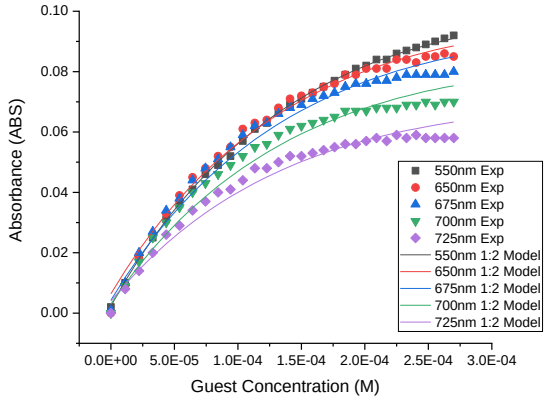

K_{a1} (M^{-1})	K_{a2} (M^{-1})
339,236 (±2.53%)	606,232 (±2.53%)

Figure 2.4: $CuBF_4$ fit initial guesses K_{a1} = 10,000 M^{-1} , K_{a2} = 50,000 M^{-1}, ϵ_{HG} = 1,000 M^{-1}, ϵ_{H2G} = 1,000 M^{-1}

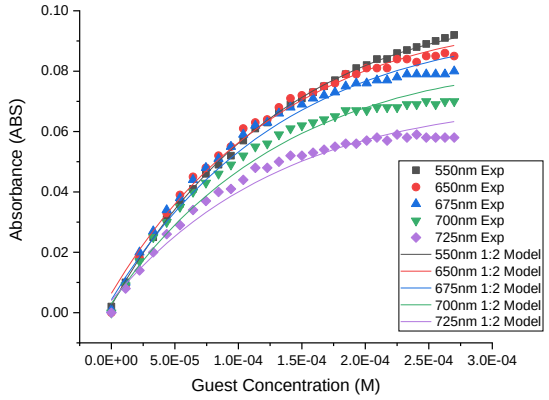

K_{a1} (M^{-1})	K_{a2} (M^{-1})
0.00124 (±13,874%)	12,524,052 (±2.58%)

Figure 2.5: $CuBF_4$ fit initial guesses K_{a1} = 1 M^{-1} , K_{a2} = 10,000 M^{-1}, ϵ_{HG} = 1,000 M^{-1}, ϵ_{H2G} = 1,000 M^{-1}

of course must be confirmed by a positive model fit to experimental data to validate the assumption of non-cooperative binding. Furthermore, an additive model assumes that the physical change during binding is additive or not, defined by $\delta_{H_2G} = 2\delta_{HG}$ or $\epsilon_{H_2G} = 2\epsilon_{HG}$. Considering all possible binding methods results in 4 distinct binding model variation for a 2:1 system, summarized by Thordarson and Hibbert.[34]

Constraining K_{a1} is important to reduce the number of fitting parameters seen in **Table 1.1** for a suspected cooperative binding. Tackling this problem with experiments was conducted in a system where copper complexes ($CuBF_4$ and $CuPF_6$) were dissolved in acetonitrile at high enough concentrations to be considered saturated, 0.5 mM, then 0.1 molar equivalents of ATF was titrated in 10 μM aliquots and absorbance was measured from 190-1100 nm. This procedure was repeated until five molar equivalents of ATF compared to copper was reached. The underlying assumption is that with such a saturated solution of copper that the initial 1:1 binding of host to guest would be favored due to the scarcity of host in the system. Starting at zero equivalents and fitting limited regions of the titration data to a 1:1 binding model, **Figure 2.6** shows an estimation of K_{a1} was possible. This estimate reduces the flexibility of the fitting parameter K_{a1} while fitting the full 2:1 binding model with experimental data by constraining its values to a region of ± 10% of the 1:1 binding model estimate. Reducing the flexibility of K_{a1} shows a significant decrease in overfitting and allows for the convergence on a global minimum error in the cost function for the 2:1 binding of ATF and copper complexes.

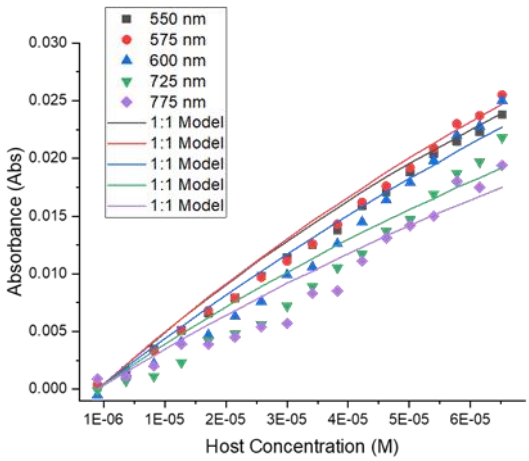

Figure 2.6: ATF titrations into saturated CuBF4 (Guest) in acetonitrile, fit to a 1:1 binding model for estimation of K_1.

2.3 Results

1:1 Binding

Optimized association constants and physical change parameters for the 1:1 binding models for Cu(I) iodide and ATF ligand are shown in **Figure 2.7**. With regards to the 1:1 binding of the ATF ligand and Cu(I) halides, coupling proton NMR and UV-Vis host:guest models shows consistency between optimal values compared to independent fitting of each

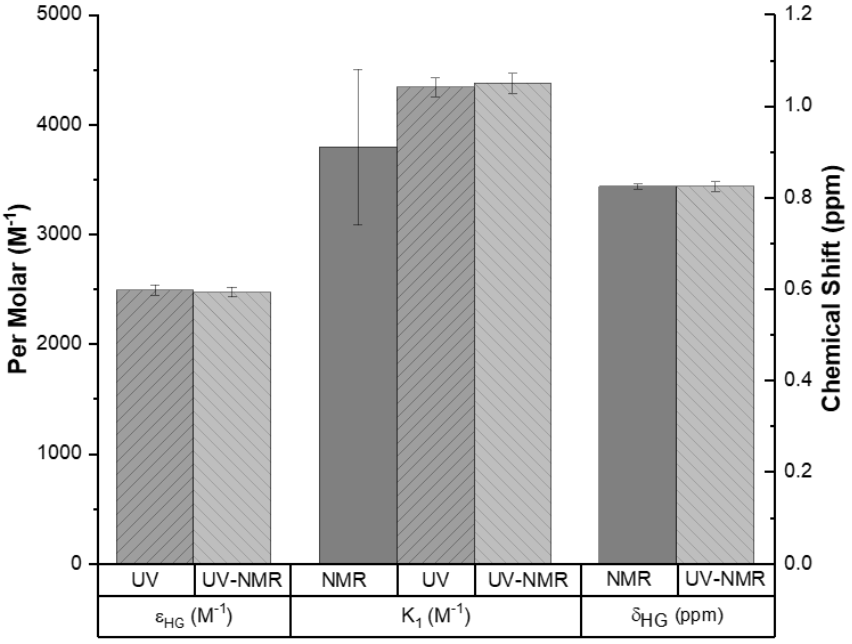

Figure 2.7: Cu(I) Iodide binding parameters fitted to a full 1:1 host:guest binding model for both coupled (UV-NMR) and independent UV/Vis (UV) and ^{1}H NMR (NMR) models.

model. It can be noted, however that the variance seen in the independent proton NMR model for the association constant is larger than the coupled UV-NMR system. Values for UV-Vis extinction coefficients were averaged at 550 nm wavelengths for triplicate titrations, similarly the chemical shift was also averaged over triplicate titrations. The observed variance in physical change values were minimal for independent and coupled 1:1 host:guest models. Overall, there is good agreement between the model predicted values across all fitting methods.

The model fits compared to experimental measurements for Cu(I) Iodide titrations into ATF can be seen in **Figure 2.8** for both independently fit UV/Vis and proton NMR binding isotherms contrast to a coupled fit with both 1:1 host:guest models fit simultaneously. Fits were obtained through reduced error for the sum of residuals described in **Eqs 2.7-9** obtaining the best fit parameters to produce the fits seen in **Figure 2.8.** Model fits are observably excellent and very consistent between fitting methods, whether independently or

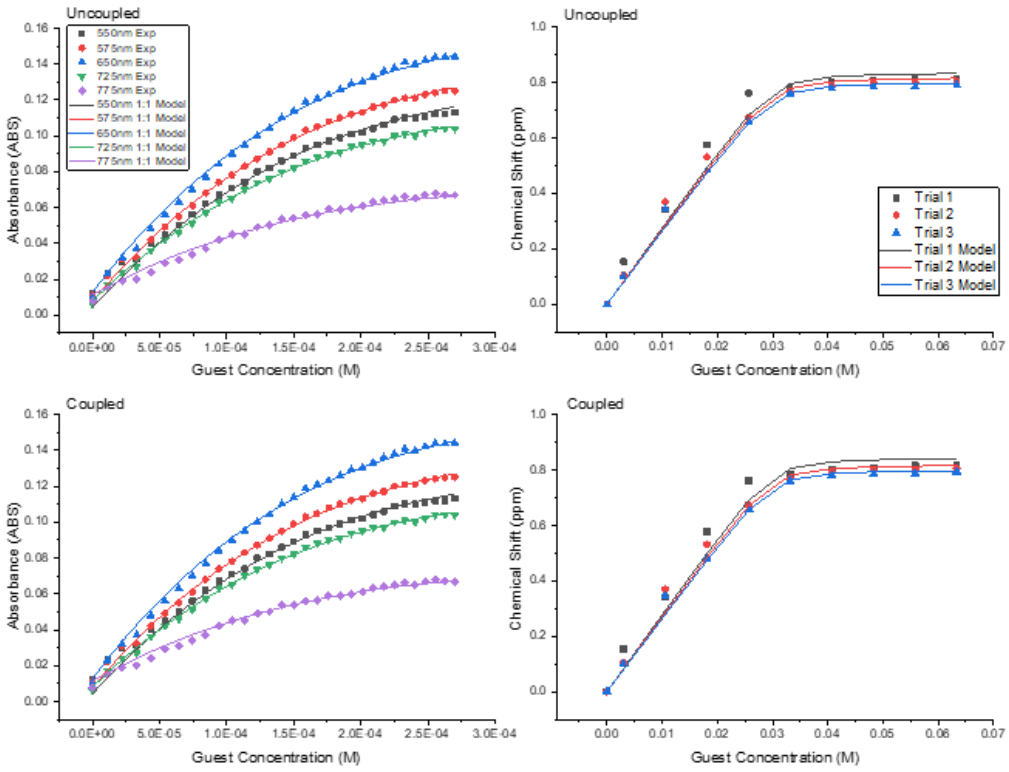

Figure 2.8: UV/Vis and ^{1}H NMR binding isotherms for titrations of Cu(I) Iodide into ATF fitted to the 1:1 host:guest binding models for UV-Vis and NMR, independently (Top) and coupled models solved simultaneously (Bottom).

simultaneously fit, both 1:1 model result in near identical goodness-of-fit. Between UV/Vis and proton NMR binding isotherms for Cu(I) halides both seem to reach a saturation point, where the concentration of the 1:1 complex approaches the concentration of total host, but distinctions can be made because saturation is achieved at different rates and at different concentrations of guest in the system. Binding isotherms for Cu(I) halides produced using UV/Vis spectroscopic measurements show a more gradual increase as saturation conditions are reached and the slope seems to depend on the wavelength of interest. Conversely, the

proton NMR binding isotherm has a relative high slope when compared to the UV/Vis binding isotherm which may lead one to assume that the association constant is higher for this system. However this can be explained by the differences in concetration values between UV/Vis and NMR, where NMR is reaching saturation much quicker due to a higher working concentration. While UV/Vis may still be trending toward full saturation it should still be linear, but because of dilution effects from titrations the absorbance will see some hinderance as the complex becomes more dilute, giving the UV/Vis binding isotherm some non-linearity.

2:1 binding

The complexity of the system increases significantly when analyzing the 2:1 binding of Cu(I)BF_4 with the ATF ligand. Determined association constants and physical parameters for the 1:1 and 2:1 complexes can be seen in **Figure 2.9** for the coupled host:guest models for UV/Vis and proton NMR, the chemical shift values for the complexes can be seen in **Figure 2.10**. The best fit values for each fitting method vary greatly depending on which binding isotherm is fitted and where or not the measurement models are fitted independent or coupled and solved simultaneously. There is a large disagreement between the UV/Vis and proton NMR association constants obtained through independent fitting to full host:guest models. When fitting the two 2:1 models for UV/Vis and proton NMR binding isotherms simultaneously as with coupled reduced error in the sum of squared residuals, and entirely different binding phenomena is described that neither independently fit model describes. When looking at the simultaneously fit 2:1 host:guest models it can be seen that the 2:1 complex is highly favored with a very large value for K_{a2} for both the Cu(I) complexes. However, the molar extinction coefficient for H_2G is very small (~200 M^{-1}) with respect to the molar extinction coefficient for HG (~18,000 M^{-1}), this trend is supported by the absorption spectra in which the regions of interest between 500 and 800 nm, associated with the complex, which shows a much more suppressed absorbance.

Additionally, the values for the extinction coefficient for HG between Cu(I) complexes and the ATF are shown to be much larger than those for the H_2G extinction coefficients. If the absorbance response, which is directly correlated to the concentration of species present in the system, is small in the wavelengths of interest it is reasonable to assume that a species with a small extinction coefficient is dominating. This observation further

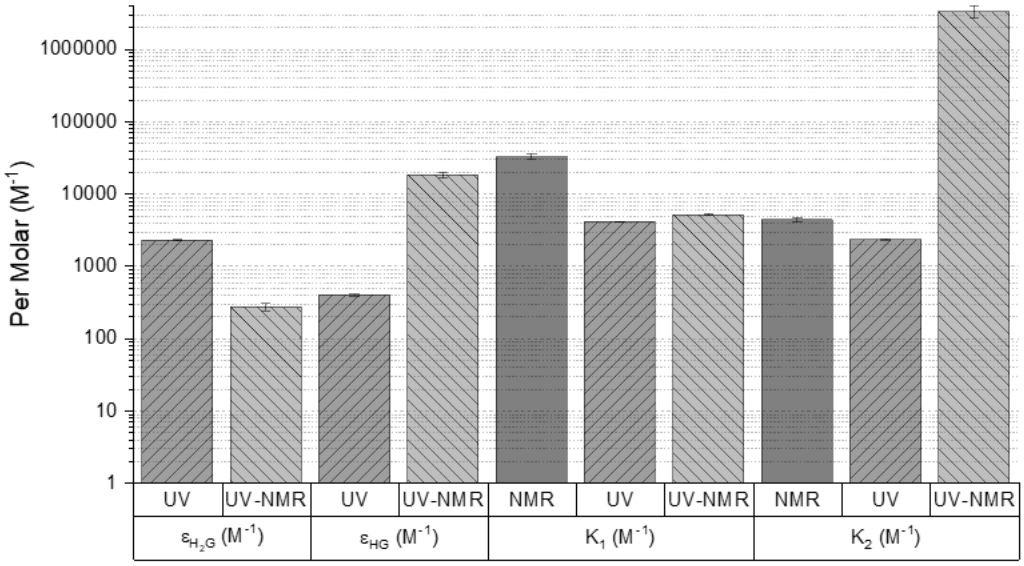

Figure 2.9: Cu(I) BF4 binding parameters fitted to a full 2:1 host:guest binding model for both coupled and independent UV/Vis and ^{1}H NMR model. Initial guesses K_{a1} = 1 M^{-1} , K_{a2} = 10,000 M^{-1}, ϵ_{HG} = 1,000 M^{-1}, ϵ_{H2G} = 1,000 M-1, $\Delta\delta_{HG}$ = 1 ppm, $\Delta\delta_{H2G}$ = 1 ppm.

corroborates the very large K_{a2} because if the system is primarily saturated with the weak absorbing H_2G one would expect a suppressed absorbance signal to be observed. Looking at the chemical shift, shown in **Figure 2.10**, an absurdly large chemical shift is determined, when fitting is done on NMR independently, outside the realm of possibility and can be considered as a model mismatch when fitting the 2:1 proton NMR binding isotherm, most likely as a result of the overfitting of the full 2:1 host:guest model. Upon coupling the UV/Vis and proton NMR model equations the chemical shifts take on much more realistic values, seen on the right side of **Figure 2.10**. Again, the physical parameter of the 1:1 complex of Cu(I)BF_4 with ATF, in this case chemical shift, is much larger that of the 2:1 value, similar to the extinction coefficients of the 1:1 complex, but because we are seeing such large affinity for the 2:1 complex this physical change contribution of the 1:1 complex has a minimal effect on the resulting binding environment and the proton NMR binding isotherm, seen in **Figure 2.11**.

The binding isotherms presented in **Figure 2.11** represents the 2:1 binding of $CuBF_4$ and the ATF ligand. Comparing the fits between the 2:1 host:guest models for UV/Vis and proton NMR, the same comparison can be made as with the 1:1 models in that the slope of the UV/Vis binding isotherm is observably smaller than that of the proton NMR slope and nonlinearity in the UV/Vis isotherm is a result of dilution effects. However, the K-values for both UV/Vis and proton NMR binding isotherms should be equal because the same binding phenomena should be occurring in both systems. Now when comparing the goodness-of-fit between the independently fit host:guest models and when models are coupled and fit simultaneously there is a noticeable difference in the goodness-of-fit with a much closer fit in the coupled models than compared to the independently fit models. Looking deeper into the

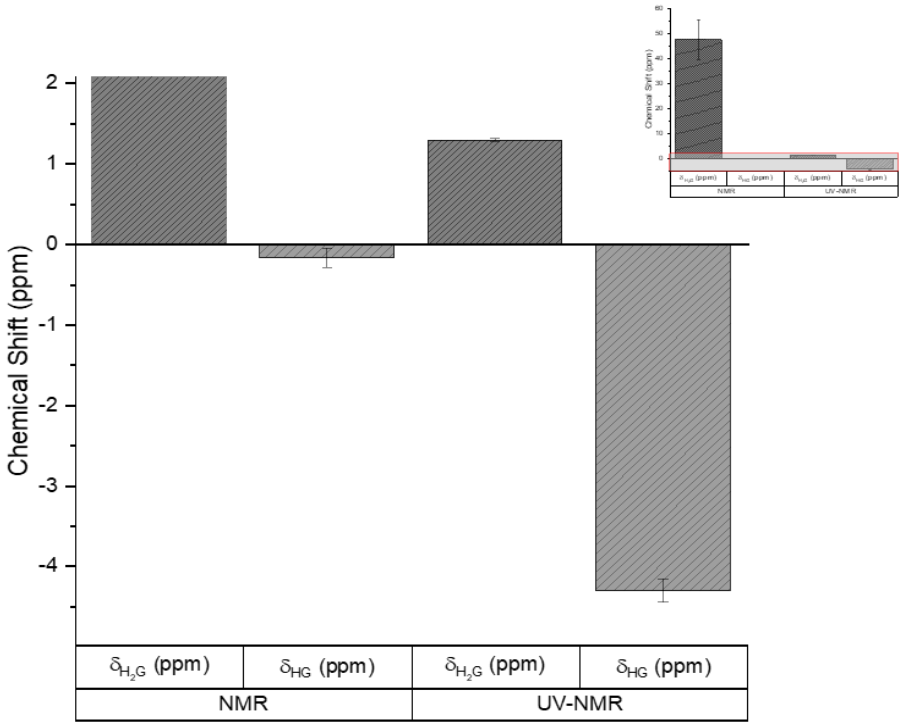

Figure 2.10: Cu(I) BF4 chemical shift parameters fitted to a full 2:1 host:guest binding model for both coupled and 1H NMR model.

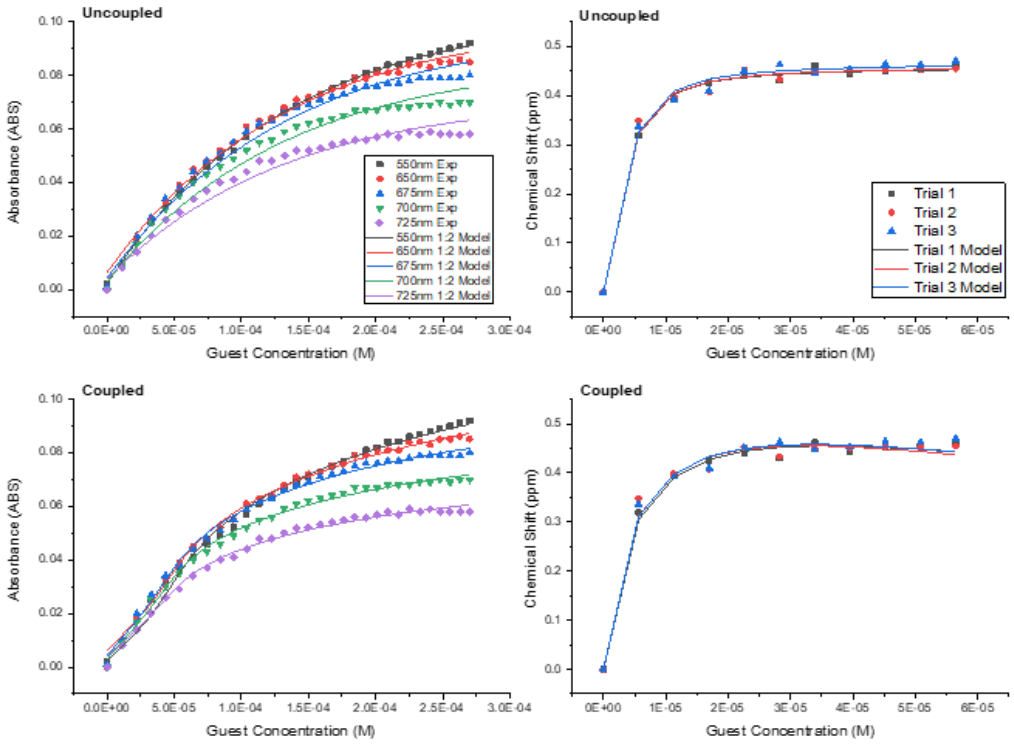

Figure 2.11:Titrations of $Cu(I)BF_4$ into ATF fit to full the 2:1 host:guest binding models for UV-Vis and ^1H NMR, independently (Top) and coupled models solved simultaneously (Bottom).

binding phenomena, when comparing the parameters of best fit shown in **Figure 2.9** and **Figure 2.10** it is surprising that the fits look similar at all, as the differences in values predicted by optimization of each case are vast. This same magnitude of difference in best fit parameters and goodness-of-fit compared to coupled host:guest models is also observed for the other Cu(I) complex, $CuPF_6$, with results presented in the appendix.

2.4 Discussion

Association constants and physical parameters may be considered reliable when the values satisfy the host:guest models independently and in simultaneously coupled systems. This secondary determination with an additional measurement method only shows that the binding is truly constant and independent of the measurement method. Because the determination of the best fit parameters is a simple case for the 1:1 host:guest binding case, due to fewer adjustable parameters during the theoretical modelling, it may be thought unnecessary to couple for 1:1 but it can be seen that there is some disagreement between

measurement methods. That is not to say that coupling the two models is not useful in the case of 1:1 binding phenomena, however it is easy to see that model coupling is needed due to the differences seen in the binding isotherms for the UV/Vis and the proton NMR. Because of the variance that occurs with proton NMR measurements the need for coupling is highlighted as a corrective effort for the association constant determination through the proton NMR host:guest model.

In the case of the 2:1 binding of host and guest the system is much more complex with many more adjustable parameters, in this context the secondary measurements are imperative for determining a reliable value for the association constant and coupling the two measurement models is highly useful. As it was presented, the 2:1 binding models are very complex with four adjustable parameters that cannot be handle by traditional linearization methods, nor should they be. The use of numerical methods is truly the only means for the determining association constants in higher order binding environments. Because there are more unknown parameters than defined equations describing the binding phenomena a numerical fitting process ultimately leads to overfitting of the system in most cases, where determined values will have no meaning and are often highly dependent on the initial guesses provided by the user.

The only way to reliably determine a association constant is to add some constraint to the system through either a secondary measurement or an assumption that defines fitting parameters in terms of each other. In the case of non-cooperative binding the association constants can be related, due to the truly identical binding sites, as a factor of four for the first association constant equal to the second association constant therefore reducing the number of adjustable fitting parameters. Additionally, if the physical change can be assumed additive then the physical change of the initial 1:1 binding phenomena can be assumed double of the physical change seen in the 2:1 binding phenomena, again reducing the number of physical parameters. These binding conditions may also occur in conjunction reducing the fitting parameters even further to the same number as 1:1 binding models, this would be considered statistical fitting. However, these assumptions must be individually fit themselves and determined valid before assuming the reliability of the best fit values for the system of Cu(I) binding to ATF in both the 1:1 and 2:1 complex it was found that the best fit occurred while

applying the full cooperative model, with all other models performing poorly, seen in the appendix. Consequently, because the binding phenomena is independent of the measurement method, the fitting model must arrive at binding values that fit both the UV/Vis and proton NMR binding isotherms, which can be determined through the coupled fitting routine described.

The true benefit of a coupled fit between multiple models with global association constants is highlighted for cooperative binding. Due to the nature of proton NMR it is unlikely that the saturated conditions needed to isolate the initial 1:1 binding phenomena are realistic, whereas in UV/Vis this can often be a convenient measurement, as a result when fitting the full 2:1 binding models independently disagreements in the determined values are almost always going to occur and as seen in the case for proton NMR can lead to unreasonable values that still provide good fit. However, if the, models are coupled together by global association constant, the constrained K_1 is applicable to both models during minimization of error, resulting in consistent values for the association constants shared by both systems and equally good fits compared to experimentally determined values. A coupled fitting model provides a tool for a more reliable determination of binding constants, for the 1:1 model coupling of NMR and UV-Vis gives confirmation of a reliable binding constant that is ambiguous from independent results and for the2:1 model coupling is a necessity for reliable determination of cooperative binding interactions

Chapter 3: Rare Earth Element Detection with Arsenazo III Ligand

The supply of rare earth elements (REE) is situated in an economically insecure state due to 90% of global demand satisfied by a near monopolized source and global demand overwhelming availability.[14–16] Necessitating the development of supply chain diversification, one method of focus for research is REE screening and recovery from waste streams or natural water sources.[17–19] The fluorometric determination of REEs bound to arsenazo-III would reach lower detection limits, compared to traditional UV/Vis spectroscopy, down to nanomolar (nM) quantities while also mitigating interfering responses from competing cations, making fluorescence an useful tool for screening waste streams for the recovery of REEs. Fluorescence scans were conducted from 5 μM down to seawater concentrations of 2 nM. Simulated seawater gave an analogous natural system that contains many competing cations, unfortunately the response of these competing cations showed a response that was either identical or more intense than that of REEs. The level of detection (LOD) and level of quantification (LOQ) was also found to be comparable to UV/Vis, making it seem that fluorescence spectroscopy is just as good at detecting REEs as traditional UV/Vis.

Although industrial waste streams typically carry low concentrations of REEs the large throughput of waste streams makes the accumulation of REEs significant.[19] However conventional methods of low level detection can be economically cumbersome with just transport and analysis alone, such as using inductively-coupled-plasma mass spectrometers (ICP-MS) the current standard for REE analysis.[58–62] Other methods for determining REEs include atomic emission spectrometry, mass spectrometry, electrothermal atomization, X-ray fluorescence analysis, and neutron activation analysis.[63,64] As well numerous preconcentration methods have been proposed to allow for measurement using liquid-liquid extraction, dispersive liquid-liquid extraction, liquid-liquid micro extraction, and solid floating drop micro-extraction.[65] In addition to liquid-liquid extraction, solid phase extraction using commercial resins, in-house resins, silica based exchange materials, and other solid materials have been researched for measuring REE.[65] Spectroscopic methods seem by far the most cost efficient compared to ICP-MS, with the ability to detect trace quantities without preconcentration.

The binding between the dye arsenazo-III has been investigated for several REE species using UV/Vis spectroscopy by Rohwer, Collier, and Hosten for defining the

coordination and stoichiometry, they did determine that arsenazo formed a 1:1 complex with several REEs, however this was conducted only in non-complex aqueous medium buffered to various pH conditions without any competing cations that could occur in field samples and the group was not investigating LOD or LOQ of the measurement.[24,66,67] Measurements using a UV-Vis spectrophotometer may not be as reliable in these more complex media due to overlapping or overshadowing absorbance peaks, at the reported measurements wavelengths 610 and 655 nm, that arise from competing cations binding to arsenazo. Fluorometric detection of REEs, using arsenazo III as a fluorometric sensitizer, may provide a more reliable method for a lower level of detection compared to UV-Vis, while reducing the chance of interference from competing cations in complex media. As well, the innovation of portable fluorometers would reduce the wait time for analysis resulting in a completely in-house low concentration detection method for REEs in natural waters or waste streams.[68] These advantages of fluorescence spectroscopy over traditional detection methods highlights the importance of establishing the LOD and LOQ for detecting trace REEs in various aqueous medium.

3.1 Methods

Reagents: Arsenazo III was purchased from Sigma Aldrich, 99.9% pure Ln-nitrate hexahydrate (where Ln = Nd, Sm, Eu) were purchased from Strem chemicals.

Fluorescence Detection

Fluorescence detection capability was tested using a Shimadzu RF-5301PC spectrofluorophotometer to measure the emission of solutions containing $Ln(NO_3)$ $\bullet nH_2O$ (where Ln = Nd, Sm, and Eu) in type 1 (18 MΩ) water saturated with the arsenazo III, as a photosensitizer, in the wavelength ranges of 220-900 nm. Starting with a stock concentration of a 500 μM REE solutions in type 1 water, dilutions were prepared from the 500uM stock into appropriate concentration step sizes of 50 μM and 5 μM. Samples were prepared through dilution of stock solutions with type 1 water and 130 μM arsenazo-III, where the total volume was kept constant at 4 mL as well as a 13 μM concentration of arsenazo to cover all REEs present on a molar basis. To maintain equilibrium in the samples and prevent the stagnation of REEs on cuvette walls, half of the 4 mL sample was initially added to a quartz cuvette (Source) prior to scans, as a wash, then dispensed before adding the remaining half of the

sample to the cuvette for measurement. Emission was observed to be most intense between 600-800 nm at excitation wavelengths between 450-700 nm, this allowed for future scans to be constrained to only look at this region.

The intensity of the response was normalized to a 0-100 scale to allow for better interpretation due to variations in the baseline measurements. Post normalization all REEs showed similar fluorescence responses when coordinating with the arsenazo ligand. Fluorescence responses to concentrations above 1 uM REEs can be seen in the appendix and were noticeable at slit lengths of 1.5 nm for emission and 5 nm for the excitation. Analyses of sub micromolar concentrations required altered slit lengths expanded to 5 nm for emission measurement and 15nm for excitation, to observe similar intensity responses for detection. After scanning in the fluorometer samples were placed in a Thermo Scientific Evolution 201 UV/Vis Spectrophotometer to record the absorbance spectra from 190-1100 nm for comparison of detection advantages.

Simulated seawater was prepared, using a common formulation by Kester, to use as an ionically complex enviorment.[69] Arsenazo will bind to cations present in the system so it was necessary to develop an optimal concentration of arsenazo in the system to ensure that all REEs present will bind to free arsenazo so that the REE-Arsenazo complex may be detected. Determination of this optimal Arsenazo concentration involved a titration study of adding Arsenazo in 0.1 mL aliquots to a simulated seawater solution of constant REE concentration. Once the optimal Arsenazo concertation was determined it can be held constant while the concertation of REEs is reduced to determine a limit of detection using fluorometric measurements. Solutions of decreasing REE concentration were prepared in seawater, at the optimal Arsenazo concentration, starting at 0.5 μM down to concentrations seen in natural seawater of about 2 nM.

3.2 Results

UV/Vis spectroscopy scans showed the sub micromolar concentration ranges were below detection limit for the REEs investigated by UV/vis. **Figure 3.1** shows the comparison between a 13 m arsenazo solution in type 1 water, on the bottom of the graph, and two different concentration samples of REEs, 1uM and 2nM, with the same concentration of arsenazo. The absorbance spectra show consistently similar absorbance responses, leading to the observation that the only species that is detected in this system is the arsenazo dye itself and the REE species present are either overshadowed by the arsenazo absorbance peaks or simply not discernably detected. In either case this result shows that UV-Vis Spectroscopy is not well suited as a detection method for the low-level detection of REEs using arsenazo as an

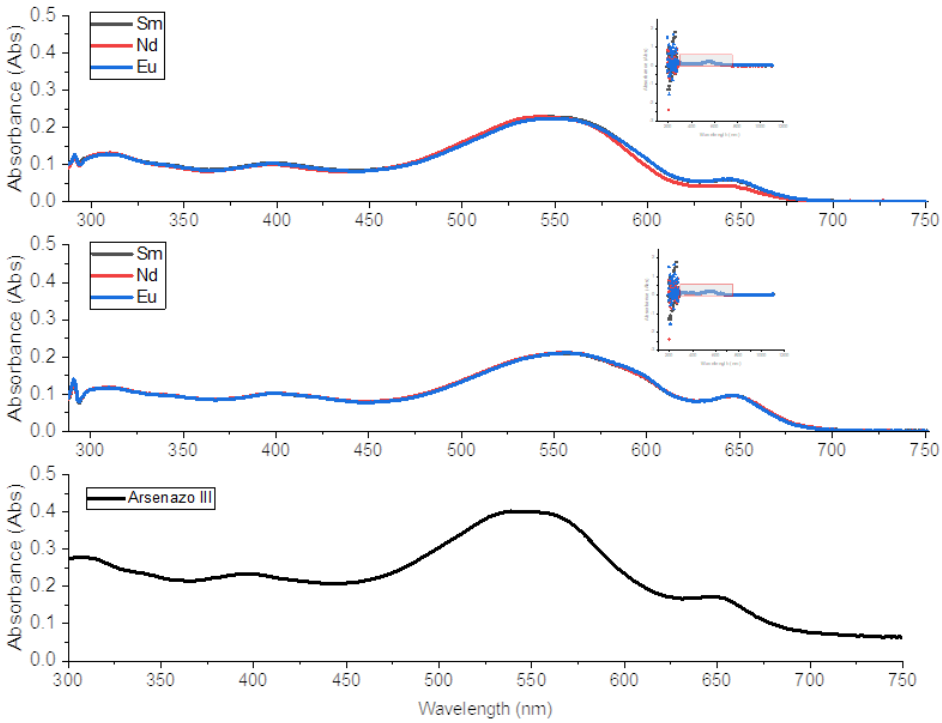

Figure 3.1: Absorbance spectra of 1uM REEs with 10% (v/v) Arsenazo III (Top), 2nM REEs with 10% (v/v) Arsenazo III (Middle), and 10% (v/v) Arsenazo III in type 1 water (Bottom).

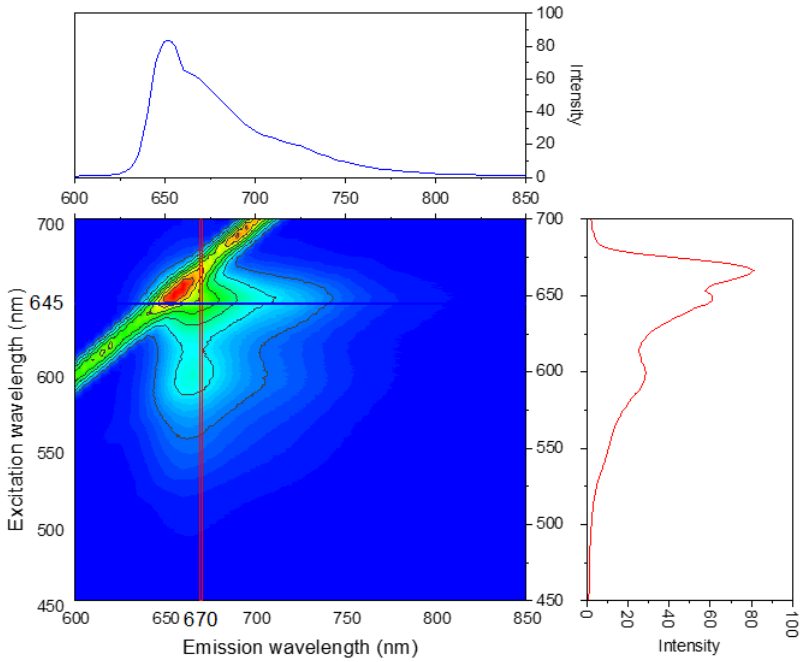

Figure 3.2: 1 μM Samarium in a 13 μM arsenazo-III solution

indicator. Fluorometric scans of REEs were able to detect the micromolar concentrations that were present at the same concentration of arsenazo as the absorbance scans with UV-Vis. The presence of arsenazo promoted a florescence response when bound to REEs. Solutions of

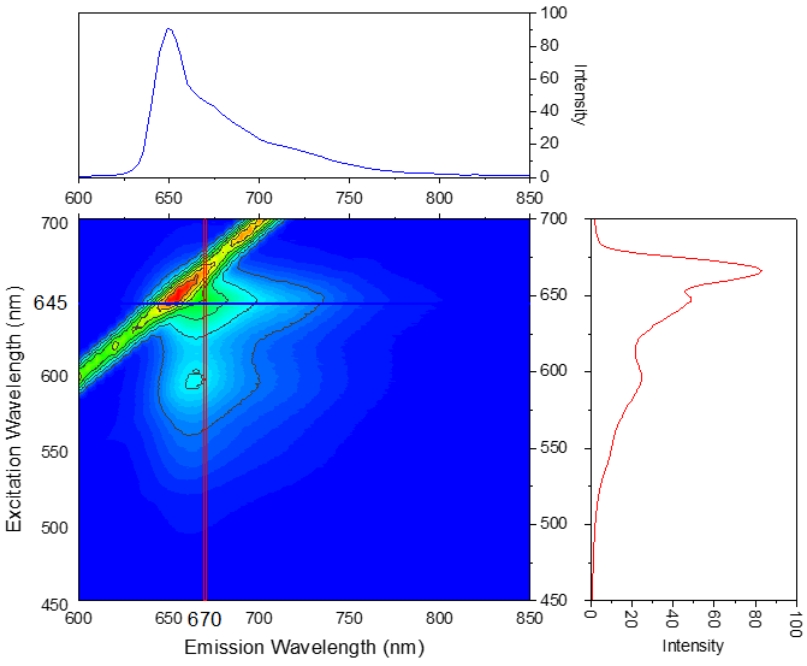

Figure 3.3: 1μM Neodymium in a 13 μM arsenazo-III solution

REEs and arsenazo prepared in type 1 water showed a significant intensity response compared to background arsenazo, shown in **Figure 3.2** for Samarium at 1uM. The detection of Europium and Neodymium are represented in **Figures 3.3-4** and are seen to have similar results. REEs complexed with arsenazo absorb between 600-700 nm and emit light most intensely between 625-700 nm adjacent the Rayleigh scatter line intersecting the top left of the fluorescence spectra. The spectra were sectioned at 670 nm emission and 645 nm

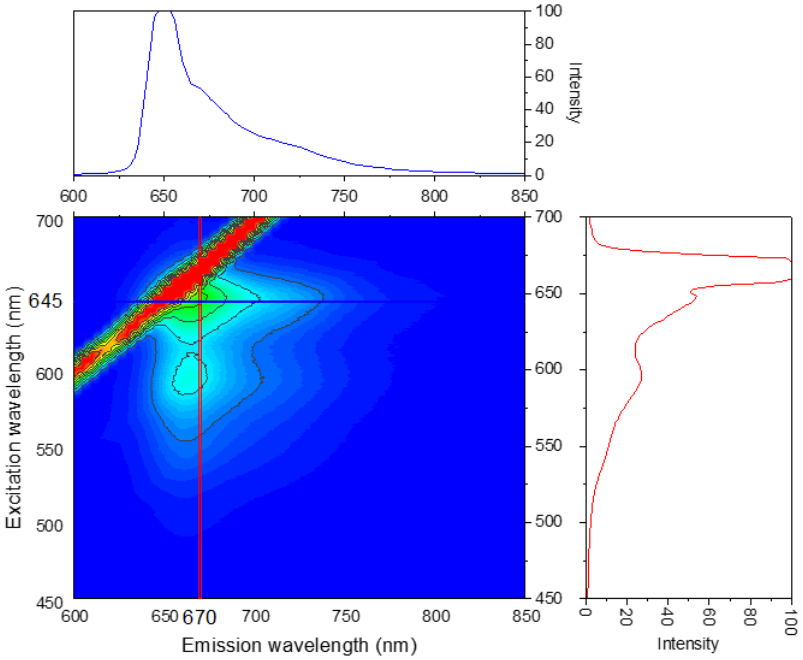

Figure 3.4: 1μM Europium in a μM arsenazo-III solution

excitation wavelength, the cross-section of the two wavelengths was chosen as the observable maximum response of the arsenazo-REE complex.

Emission spectra is shown to the right of the figure, plotted over excitation wavelengths as a function of intensity, next to the maximum peak associated with the Rayleigh scatter line there are two distinct intensity peak that can be associated with the complex and the highest occurs at the cross-section wavelength 635 nm. Similarly, in the excitation spectra there is a distinct peak at the cross-section peak for 670 nm emission wavelength. Looking at all REEs investigated this trend is consistent for all emission and excitation spectra plotted, indicating similar complexes. Upon dilution in type 1 water while keeping a constant arsenazo concentration, to ensure that light attenuation was not altering the fluorescence signal, several concentrations were measured from 1 μM to 2 nM. **Figure 3.5** represents the linear fit of

concentration as a function of intensity and absorbance for neodymium, as the representative REE, with average R-square value greater than 0.95, when the intercept is not fixed at zero. After dilutions of REEs were conducted, it was observed that detection was comparable with that of UV/Vis spectroscopy. Unfortunately, the responses seen just below 1.6 μM were determined to be below the lower detectable limit, calculated as three standard deviations above the average background fluorescent signal produced by the 13 μM Arsenazo blank.[70] This would indicates that the presence of REEs below the LOD concentrations are not detectable from the background interference. **Figure 18** shows the region of detectability occurring at 1.6 μM for fluorescence and 1.4 μM for UV/Vis absorbance.

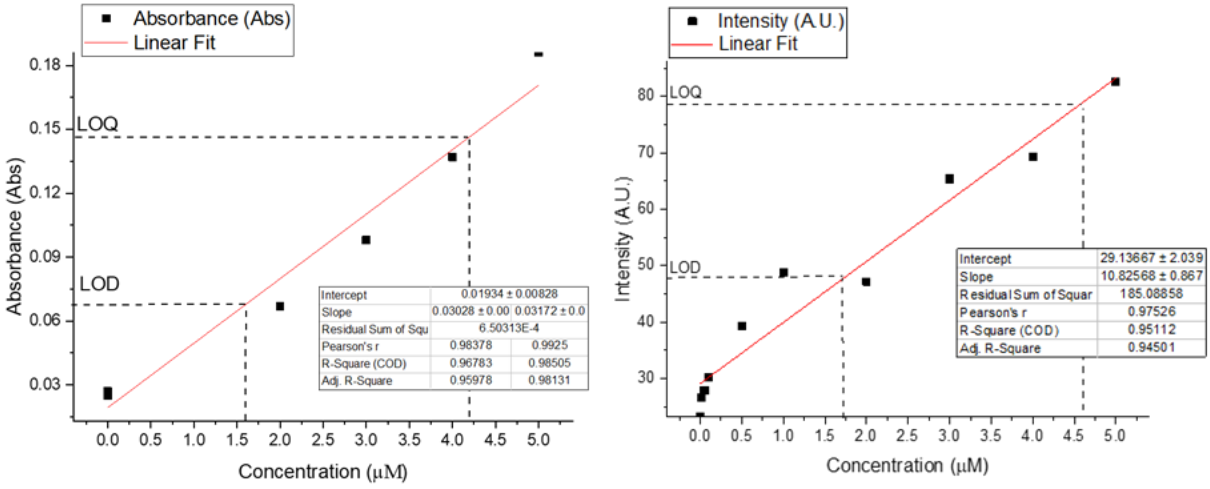

Figure 3.5: Linear fit between Absorbance and μM concentrations of Neodymium (left). Linear fit between fluorescence intensity and μM concentrations of Neodymium. (A.U): Arbitrary Units

Once the fluorometric detection of REEs was found to comparable with UV/Vis, type 1 water was replaced with simulated seawater to investigate the hypothesis that fluorescence has reduced overlap in spectra from competing cations. Initial scans of samples containing only seawater and arsenazo were conducted to determine if the simulated seawater would fluoresce independently of the REEs. It was observed that the simulated seawater did fluoresce without the addition of REEs and in the same wavelengths for excitation and emission, likely due to arsenazo binding to the large cations present in the system. Comparison scans of seawater containing 1 μM concentrations of REEs in Arsenazo were shown to have little difference to the fluorescence scans of samples containing only seawater which would not allow for detection of REEs specifically in a complex cationic system. Further investigation

showed that the fluorescence response of seawater was largely due to the arsenazo complexation with strontium and calcium cations present in the simulated seawater, shown in **Figure 3.5**, as well magnesium had a weak fluorescence response with Arsenazo.

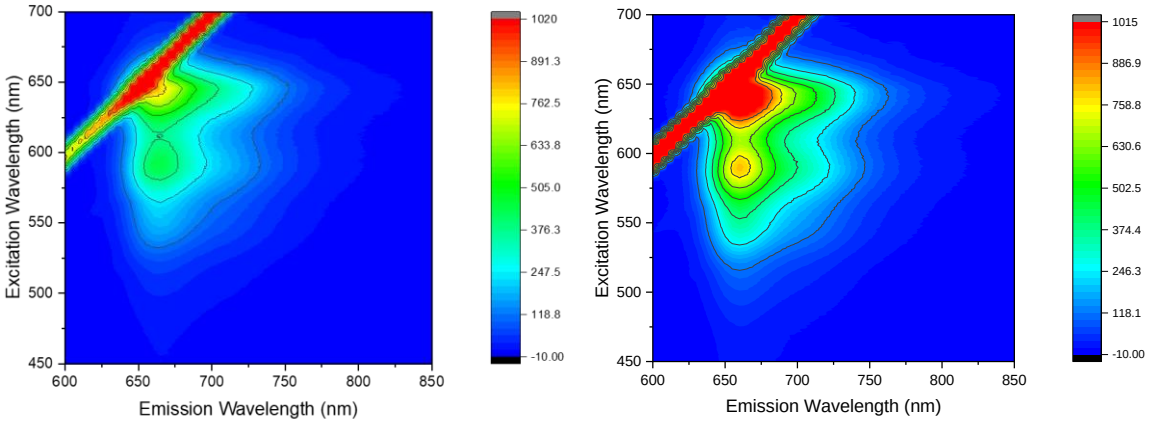

Figure3.6: Fluorescence response of aqueous $CaCl_2$ (left) and $SrCO_3$ (right) in 13 μM arsenazo solutions.

3.3 Discussion

The ultra-trace detection limit of REEs using fluorescence is currently much higher than ICP methods for detect limits.[59,60] However, fluorescence shows great promise in the ability to determine REEs in aqueous waste streams, with an absence of competing cations, and additional paths for improving detection may lower the detectable limit even further. The usefulness of portable fluorometers for determining alternative sources for REEs would still be beneficial as a screening method for on-site waste stream or natural water systems evaluation as source of REEs. Industrial waste streams specifically would benefit from a faster method of determination where the accumulation of REEs in the waste stream over time results in a loss of expensive metals that can may remediated to reduce large costs through REE recovery. Considerations for improving the detection of REEs include investigating other commonly used binding fluorophore ligands and refining the fluorescence scans to reduce the variance between background arsenazo intensity, which would lower the LOD and LOQ values. A desirable ligand would have a more suppressed fluorescence response when unbound in aqueous solutions and would be less selective for cations present in seawater samples, unfortunately this would be a difficult screening process. Additionally, there are a multitude of already established preconcentration methods for REE samples that may be employed prior to running detection methods that may be an effective pretreatment prior to detection measurements with fluorescence to reduce the concentration of competing cations and improve REE detection using Arsenazo.[65] Overall, fluorescence shows promise as an alternative low-cost portable method for the quick determination of REEs present in aqueous waste streams that rivals current sample and send methods with high associated costs that include the shipping, testing, and potential losses of inaction as REEs are lost between sampling, detection, and decision to recovery REEs.

Chapter 4: Recommendations and Future Work

With a model analysis for both the 1:1 and 2:1 interaction of host and guest, investigations into the extent of both models would be beneficial for establishing the validity of the determined parameter, via the development of a master curve. The most immediate opportunity for investigation is completing NMR titrations with Cu(I) chloride to observe the interaction with another Cu(I) halide. Another Cu(I) halide experiment would show what interaction, if any, the halide participates in during complexation Continuing on from Cu(I) salts, the investigation into how the ATF ligand would bind with Cu(II) salts could be a valuable secondary study for further investigations into how the redox active ligand behaves in the presence of alternate charged species, and the reduction mechanism of either the ligand reducing prior to binding, or visa versa the reduction of Cu(II) prior to binding. Along with Cu(II) salts it would be worthwhile to investigate the binding of ATF with other transition metals such as the metals reported in the original work done by Neilson and Bechgaard, including Pd, Pt, and Ni, as these transition metals can exist in higher oxidation states than Cu which may result in different coordinated complexes with ATF.[22] Going further it is recommended to pursue the binding behavior of ATF with Fe, due to a very wide range of oxidation states. As well, it would be worth while to reduce the ligand itself prior to binding to investigate the behavior of a reduced ligand when binding to Cu(I) or Cu(II) species, possibly other metals as well.

Another path for investigation would be the functionalization of the ATF ligand for the possibility of tailor made ligands that can have a broad range of functions through the tuning of the molecular electronics and steric effects, when it comes to metal scavenging chemistry. In conjunction with the functionalization of the ATF ligand it is recommended to take advantage of computational molecular modelling software for the screening of possible ligand conformations to revise the charge distribution and stability of functionalized molecules before performing synthesis techniques at the expense of reagents and time. Looking into the process of separating the ligand from bound metals would be advised regarding metal recovery through methods available in electrochemistry.

Fluorometric detection of rare earth elements requires a secondary investigation into the purity of the reagents used in the study, because of the low operating concentrations, trace contaminations of REEs in the reagents may give a false positive response. Additionally, a

fine scanning of the baseline arsenazo spectra could lower the variance in intensity values, lowering the LOD and LOQ for fluorometric detection.

References

1. Li, G. *et al.* Elemental Impurities in Pharmaceutical Excipients. *J. Pharm. Sci.* **104,** 4197–4206 (2015).
2. Al-Saleh, I. & Al-Enazi, S. Trace metals in lipsticks. *Toxicol. Environ. Chem.* **93,** 1149–1165 (2011).
3. Lee, S.-M., Jeong, H.-J. & Chang, I. S. Simultaneous determination of heavy metals in cosmetic products. *J. Cosmet. Sci.* **59,** 441–448 (2008).
4. Bocca, B., Pino, A., Alimonti, A. & Forte, G. Toxic metals contained in cosmetics: A status report. *Regul. Toxicol. Pharmacol.* **68,** 447–467 (2014).
5. Bettinelli, M., Spezia, S., Baroni, U. & Bizzarri, G. Determination of Trace-Elements in Fuel Oils by Inductively-Coupled Plasma-Mass Spectrometry After Acid Mineralization of the Sample in a Microwave-Oven. *J. Anal. At. Spectrom.* **10,** 555–560 (1995).
6. Lum, Y. *et al.* Trace Levels of Copper in Carbon Materials Show Significant Electrochemical CO2 Reduction Activity. *Acs Catal.* **6,** 202–209 (2016).
7. Nikiforov, M. P. *et al.* Detection and role of trace impurities in high-performance organic solar cells. *Energy Environ. Sci.* **6,** 1513–1520 (2013).
8. Singh, J. International conference on harmonization of technical requirements for registration of pharmaceuticals for human use. *J. Pharmacol. Pharmacother.* **6,** 185 (2015).
9. Flores, L. M. Elemental Impurities in Drug Products Guidance for Industry. 11
10. Antunes, E. F. *et al.* Analyses of residual iron in carbon nanotubes produced by camphor/ferrocene pyrolysis and purified by high temperature annealing. *Appl. Surf. Sci.* **257,** 8038–8043 (2011).

11. Edwards, E. R., Antunes, E. F., Botelho, E. C., Baldan, M. R. & Corat, E. J. Evaluation of residual iron in carbon nanotubes purified by acid treatments. *Appl. Surf. Sci.* **258,** 641–648 (2011).
12. Leadbeater, N. E. Cross coupling: When is free really free? *Nat. Chem.* **2,** 1007–1009 (2010).
13. Kim, H. & Sigmund, W. Iron particles in carbon nanotubes. *Carbon* **43,** 1743–1748 (2005).
14. Wang, X. *et al.* China's Rare Earths Production Forecasting and Sustainable Development Policy Implications. *Sustainability* **9,** 1003 (2017).
15. Zhu, K., Zhao, S., Yang, S., Liang, C. & Gu, D. Where is the way for rare earth industry of China: An analysis via ANP-SWOT approach. *Resour. Policy* **49,** 349–357 (2016).
16. McLellan, B. C., Corder, G. D. & Ali, S. H. Sustainability of Rare Earths—An Overview of the State of Knowledge. *Minerals* **3,** 304–317 (2013).
17. Sinha, S., Abhilash, Meshram, P. & Pandey, B. D. Metallurgical processes for the recovery and recycling of lanthanum from various resources-A review. *Hydrometallurgy* **160,** 47–59 (2016).
18. Westerhoff, P. *et al.* Characterization, Recovery Opportunities, and Valuation of Metals in Municipal Sludges from US Wastewater Treatment Plants Nationwide. *Environ. Sci. Technol.* **49,** 9479–9488 (2015).
19. Rozelle, P. L. *et al.* A Study on Removal of Rare Earth Elements from U.S. Coal Byproducts by Ion Exchange. *Metall. Mater. Trans. E-Mater. Energy Syst.* **3,** 6–17 (2016).

20. Nielsen, K. T., Harris, P., Bechgaard, K. & Krebs, F. C. Structural study of four complexes of the M-N2S2 type derived from diethylphenylazothioformamide and the metals palladium, platinum, copper and nickel. *Acta Crystallogr. Sect. B-Struct. Sci.* **63,** 151–156 (2007).
21. Nielsen, K. T., Bechgaard, K. & Krebs, F. C. Removal of Palladium Nanoparticles from Polymer Materials. *Macromolecules* **38,** 658–659 (2005).
22. Nielsen, K. T., Bechgaard, K. & Krebs, F. C. Effective removal and quantitative analysis of Pd, Cu, Ni, and Pt catalysts from small-molecule products. *Synth.-Stuttg.* 1639–1644 (2006). doi:10.1055/s-2006-926453
23. Rowatt, E. & Williams, R. The Interaction of Cations with the Dye Arsenazo .3. *Biochem. J.* **259,** 295–298 (1989).
24. Rohwer, H., Collier, N. & Hosten, E. Spectrophotometric study of arsenazo III and its interactions with lanthanides. *Anal. Chim. Acta* **314,** 219–223 (1995).
25. Anslyn, E. V. & Dougherty, D. A. *Modern Physical Organic Chemistry*. (University Science Books, 2006).
26. Lehn Jean-Marie. Supramolecular Chemistry—Scope and Perspectives Molecules, Supermolecules, and Molecular Devices (Nobel Lecture). *Angew. Chem. Int. Ed. Engl.* **27,** 89–112 (2003).
27. Cram, D. & Cram, J. Host-Guest Chemistry. *Science* **183,** 803–809 (1974).
28. Kyba, E. P. *et al.* Host-guest complexation. 1. Concept and illustration. *J. Am. Chem. Soc.* **99,** 2564–2571 (1977).
29. Bunn, H. F. (Howard F., 1935-, Forget, B. G. & 1939-. *Hemoglobin--molecular, genetic, and clinical aspects*. (W.B. Saunders Co., 1986).

30. Pedersen, C. J. Cyclic polyethers and their complexes with metal salts. *J. Am. Chem. Soc.* **89,** 7017–7036 (1967).
31. Thordarson, P. Determining association constants from titration experiments in supramolecular chemistry. *Chem Soc Rev* **40,** 1305–1323 (2011).
32. Hirose, K. A Practical Guide for the Determination of Binding Constants. *J. Incl. Phenom. Macrocycl. Chem.* **39,** 193–209 (2001).
33. Hargrove, A. E., Zhong, Z., Sessler, J. L. & Anslyn, E. V. Algorithms for the determination of binding constants and enantiomeric excess in complex host : guest equilibria using optical measurements. *New J. Chem.* **34,** 348–354 (2010).
34. Brynn Hibbert, D. & Thordarson, P. The death of the Job plot, transparency, open science and online tools, uncertainty estimation methods and other developments in supramolecular chemistry data analysis. *Chem Commun* **52,** 12792–12805 (2016).
35. Talib, Z. A. *et al.* Frequency Behavior of a Quartz Crystal Microbalance (Qcm) in Contact with Selected Solutions. *Am. J. Appl. Sci.* **3,** 1853–1858 (2006).
36. Kadam, S. A., Haav, K., Toom, L., Haljasorg, T. & Leito, I. NMR Method for Simultaneous Host-Guest Binding Constant Measurement. *J. Org. Chem.* **79,** 2501–2513 (2014).
37. Benesi, H. A. & Hildebrand, J. H. A Spectrophotometric Investigation of the Interaction of Iodine with Aromatic Hydrocarbons. *J. Am. Chem. Soc.* **71,** 2703–2707 (1949).
38. Lineweaver, H. & Burk, D. The Determination of Enzyme Dissociation Constants. *J. Am. Chem. Soc.* **56,** 658–666 (1934).
39. Scott, R. L. Some comments on the Benesi-Hildebrand equation. *Recl. Trav. Chim. Pays-Bas* **75,** 787–789 (2010).

40. Hanes, C. S. Studies on plant amylases: The effect of starch concentration upon the velocity of hydrolysis by the amylase of germinated barley. *Biochem. J.* **26,** 1406–1421 (1932).
41. Haldane, J. B. S. Graphical Methods in Enzyme Chemistry. *Nature* **179,** 832 (1957).
42. Scatchard George. The attractions of proteins for small molecules and ions. *Ann. N. Y. Acad. Sci.* **51,** 660–672 (2006).
43. Job, P. Formation and stability of inorganic complexes in solution. *Ann. Chim. Appl.* **9,** 113–203 (1928).
44. Ulatowski, F., Dąbrowa, K., Bałakier, T. & Jurczak, J. Recognizing the Limited Applicability of Job Plots in Studying Host–Guest Interactions in Supramolecular Chemistry. *J. Org. Chem.* **81,** 1746–1756 (2016).
45. Chemler, S. R. Copper catalysis in organic synthesis. *Beilstein J. Org. Chem.* **11,** 2252–2253 (2015).
46. Karlsson, H. L., Cronholm, P., Gustafsson, J. & Möller, L. Copper Oxide Nanoparticles Are Highly Toxic: A Comparison between Metal Oxide Nanoparticles and Carbon Nanotubes. *Chem. Res. Toxicol.* **21,** 1726–1732 (2008).
47. Ward, M. D. & McCleverty, J. A. Non-innocent behaviour in mononuclear and polynuclear complexes: consequences for redox and electronic spectroscopic properties. *J Chem Soc Dalton Trans* 275–288 (2002). doi:10.1039/B110131P
48. Luca, O. R. & Crabtree, R. H. Redox-active ligands in catalysis. *Chem Soc Rev* **42,** 1440–1459 (2013).
49. Lyaskovskyy, V. & de Bruin, B. Redox Non-Innocent Ligands: Versatile New Tools to Control Catalytic Reactions. *ACS Catal.* **2,** 270–279 (2012).

50. Berben, L. A., de Bruin, B. & Heyduk, A. F. Non-innocent ligands. *Chem Commun* **51,** 1553–1554 (2015).
51. Zhu, D., Thapa, I., Korobkov, I., Gambarotta, S. & Budzelaar, P. H. M. Redox-Active Ligands and Organic Radical Chemistry. *Inorg. Chem.* **50,** 9879–9887 (2011).
52. Bechgaard, K. Nonplanar Electron-Transfer Complexes .2. Chemistry of 4 Cu-N2s2z Complexes Derived from Copper-Bis-N,n-Diethylphenylazothioformamide. *Acta Chem. Scand. Ser. -Phys. Inorg. Chem.* **31,** 683–688 (1977).
53. Johnson, N. A. *et al.* Deconvoluting the Innocent vs. Non-Innocent Behavior of N,N-Diethylphenylazothioformamide Ligands with Copper Sources. *Eur. J. Inorg. Chem.* 5576–5581 (2017). doi:10.1002/ejic.201701097
54. Motulsky, H. J. & Ransnas, L. A. Fitting curves to data using nonlinear regression: a practical and nonmathematical review. *FASEB J.* **1,** 365–374 (1987).
55. Motulsky, H. & Christopoulos, A. Fitting Models to Biological Data using Linear and Nonlinear Regression. 351
56. Schittkowski, K. NLPQL: A fortran subroutine solving constrained nonlinear programming problems. *Ann. Oper. Res.* **5,** 485–500 (1986).
57. Cardano, G., Witmer, T. R. & Ore, O. *The Rules of Algebra: Ars Magna*. (Dover Publications, 2007).
58. Tsygankova, A., Lundovskaya, O. & Saprykin, A. Analysis of Europium, Yttrium and Lanthanum Compounds by Atomic Emission Spectrometry with Inductively Coupled Plasma. *J. Anal. Chem.* **71,** 179–184 (2016).

59. Hassan, J., Zari, N. & Tabar-Heydar, K. Determination of Rare earth elements in environmental samples by solid phase extraction ICP OES. *J. Anal. Chem.* **71,** 365–371 (2016).

60. Li, Y. *et al.* Determination of ultra-trace rare earth elements in high-salt groundwater using aerosol dilution inductively coupled plasma-mass spectrometry (ICP-MS) after iron hydroxide co-precipitation. *Microchem. J.* **126,** 194–199 (2016).

61. Li, F. *et al.* Simultaneous determination of trace rare-earth elements in simulated water samples using ICP-OES with TODGA extraction/back-extraction. *PLoS ONE* **12,** (2017).

62. Zhu, Z. & Zheng, A. Fast Determination of Yttrium and Rare Earth Elements in Seawater by Inductively Coupled Plasma-Mass Spectrometry after Online Flow Injection Pretreatment. *Molecules* **23,** 489 (2018).

63. Gorbatenko, A. A. & Revina, E. I. A review of instrumental methods for determination of rare earth elements. *Inorg. Mater.* **51,** 1375–1388 (2015).

64. Zawisza, B. *et al.* Determination of rare earth elements by spectroscopic techniques: a review. *J. Anal. At. Spectrom.* **26,** 2373–2390 (2011).

65. Fisher, A. & Kara, D. Determination of rare earth elements in natural water samples - A review of sample separation, preconcentration and direct methodologies. *Anal. Chim. Acta* **935,** 1–29 (2016).

66. Jauberty, L. *et al.* Optimization of the arsenazo-III method for the determination of uranium in water and plant samples. *Talanta* **115,** 751–754 (2013).

67. Konstantinou, M. & Pashalidis, I. Speciation and spectrophotometric determination of uranium in seawater. *Mediterr. Mar. Sci.* **5,** 55–60 (2004).

68. FluoroSELECT^{TM} single channel fluorometer Z805491. *Sigma-Aldrich* Available at: https://www.sigmaaldrich.com/catalog/product/sial/z805491. (Accessed: 8th May 2018)

69. Kester, D., Duedall, I., Connors, D. & Pytkowicz, R. Preparation of Artificial Seawater. *Limnol. Oceanogr.* **12,** 176-+ (1967).

70. MacDougall, D., Crummett, W. B. & et al., . Guidelines for data acquisition and data quality evaluation in environmental chemistry. *Anal. Chem.* **52,** 2242–2249 (1980).

Appendix

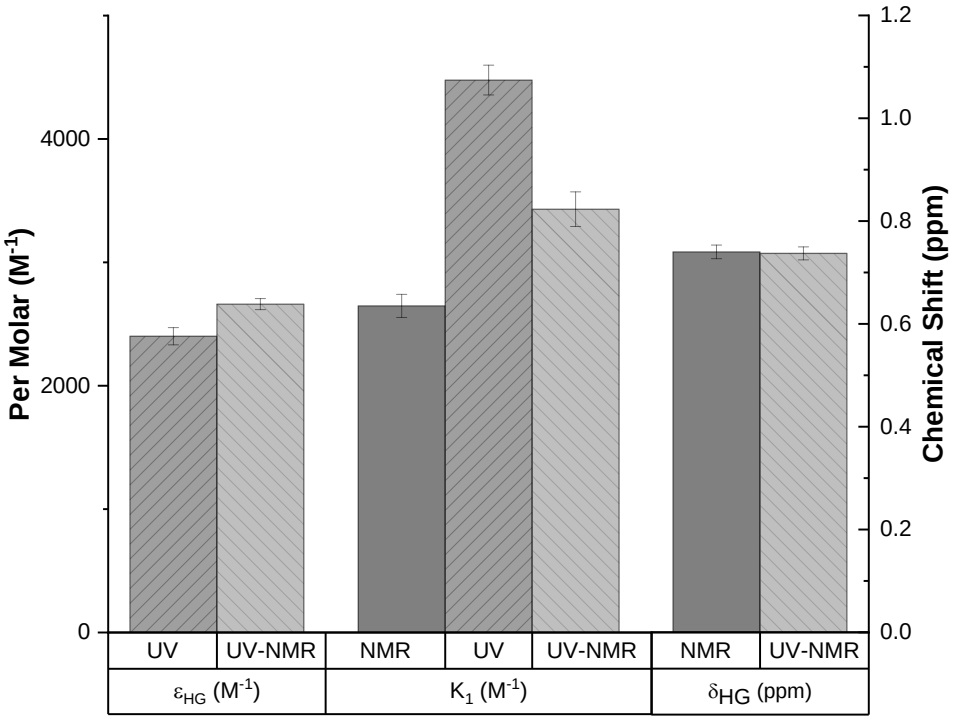

Figure A.1: Cu(I) Bromide binding parameters fitted to a full 1:1 host:guest binding model for both coupled and independent UV/Vis and ^{1}H NMR model.

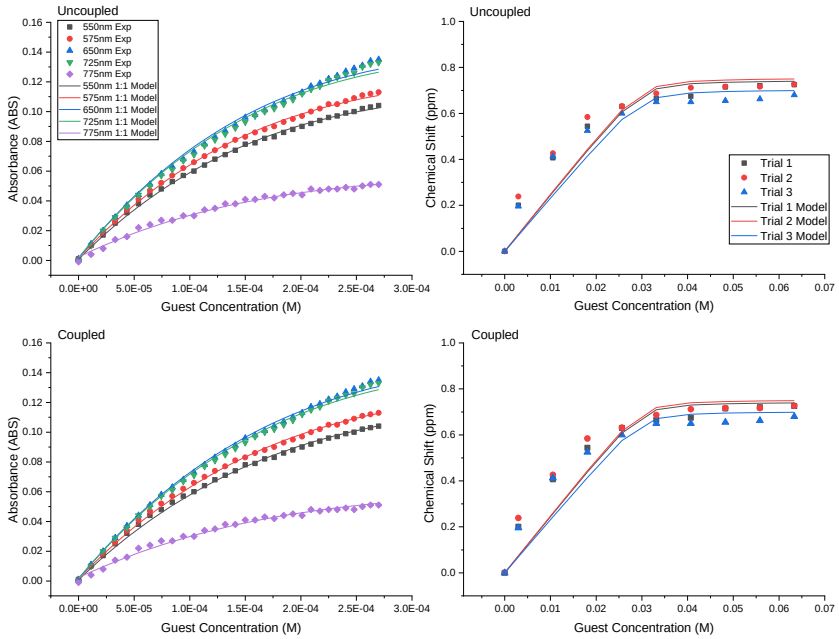

Figure A.2: UV/Vis and ^{1}H NMR binding isotherms for titrations of Cu(I) Bromide into ATF fitted to the 1:1 host:guest biding binding models for UV-Vis and NMR, independently (Top) and coupled models solved simultaneously (Bottom).

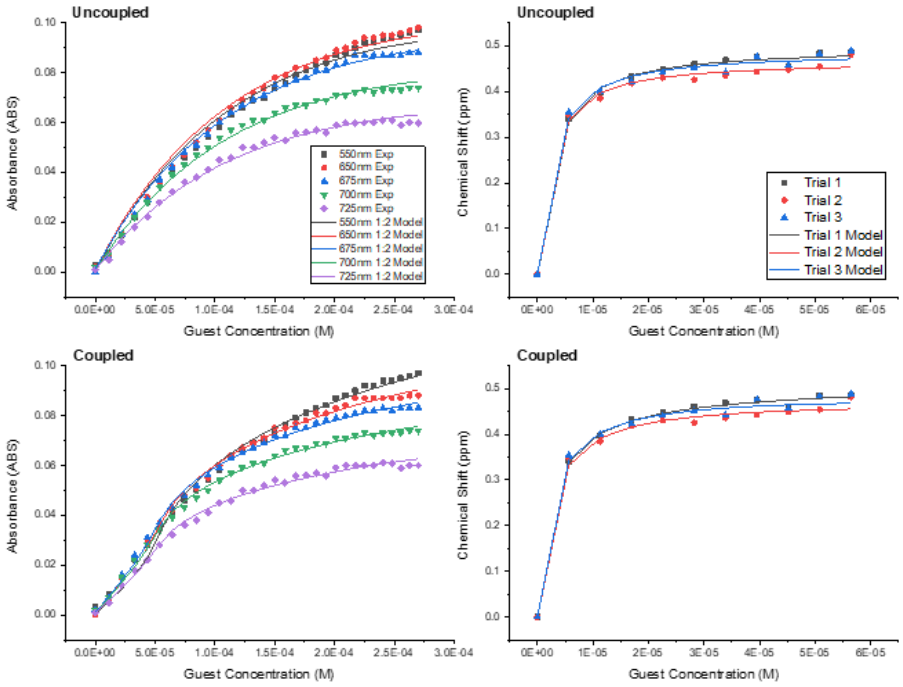

Figure A.3: Titrations of Cu(I)PF_6 into ATF fit to full the 2:1 host:guest binding models for UV-Vis and NMR, independently (Top) and coupled models solved simultaneously (Bottom).

Table A.1: Uncoupled full 2:1 host:guest model fits for UV-Vis and ^{1}H NMR. Initial guesses: K_{a1} = 1000 M^{-1} , K_{a2} = 5000 M^{-1}, ϵ_{HG} = 1000 M^{-1}, ϵ_{H2G} = 1000 M^{-1}, δ_{HG} = 1 ppm, and δ_{H2G} = 1 ppm.

	Uncoupled UV-Vis					Uncoupled ^{1}H NMR				
$CuPF_6$	K_{a1} (M^{-1})	K_{a2} (M^{-1})	λ (nm)	ϵ_{HG} (M^{-1})	ϵ_{H_2G} (M^{-1})	K_{a1} (M^{-1})	K_{a2} (M^{-1})	Trial	δ_{HG} (ppm)	δ_{H_2G} (ppm)
	275,299 (±2.52%)	590,820 (±2.53%)	550	1,855 (±1.68%)	191 (±7.81%)	369,614 (±59.7%)	185,710 (±304%)	1	0.491 (±1.62%)	0.688 (±38.4%)
			575	1,880 (±1.52%)	210 (±5.52%)			2	0.464 (±1.69%)	0.760 (±34.0%)
			650	1,696 (±1.11%)	241 (±3.91%)			3	0.480 (±1.62%)	0.746 (±35.2%)
			735	1,372 (±0.679%)	256 (±7.73%)					
			775	1,140 (±0.688%	207 (±7.68%)					
$CuBF_4$	K_{a1} (M^{-1})	K_{a2} (M^{-1})	λ (nm)	ϵ_{HG} (M^{-1})	ϵ_{H_2G} (M^{-1})	K_{a1} (M^{-1})	K_{a2} (M^{-1})	Trial	δ_{HG} (ppm)	δ_{H_2G} (ppm)
	1,165,195 (±2.53%)	6,265,785 (±2.53%)	550	2,312 (±0.654%)	221 (±1.70%)	484,106 (±3.98)	125,413 (±4.63)	1	0.109 (±2.31%)	4.31 (±150%)
			575	2.372 (±0.640%)	238 (±1.60%)			2	0.113 (±2.43%)	4.42 (±121%)
			650	2,139 (±0.567%)	267 (±0.987%)			3	0.105 (±2.18%)	4.25 (±143%)
			735	1,681 (±0.395%)	270 (±0.637%)					
			775	1,417 (±0.402%)	229 (±0.60%)					

Table A.2: Uncoupled full 2:1 host:guest model fits for UV-Vis and ^{1}H NMR. Initial guesses: K_{a1} = 10000 M^{-1} , K_{a2} = 50000 M^{-1}, ϵ_{HG} = 1000 M^{-1}, ϵ_{H2G} = 1000 M^{-1}, δ_{HG} = 1 ppm, and δ_{H2G} = 1 ppm.

	Uncoupled UV-Vis					Uncoupled ^{1}H NMR				
$CuPF_6$	K_{a1} (M^{-1})	K_{a2} (M^{-1})	λ (nm)	ϵ_{HG} (M^{-1})	ϵ_{H_2G} (M^{-1})	K_{a1} (M^{-1})	K_{a2} (M^{-1})	Trial	δ_{HG} (ppm)	δ_{H_2G} (ppm)
	1,147,124 (±2.52%)	6,266,605 (±2.53%)	550	2,543 (±0.702%)	193 (±2.54%)	73,149 (±75.6%)	15,973 (±96.8%)	1	0. 359 (±2.33%)	6.60 (±4.90%)
			575	2,573 (±0.666%)	211 (±2.12%)			2	0. 330 (±2.47%)	6.56 (±4.79%)
			650	2,304 (±0.575%)	239 (±1.21%)			3	0. 352 (±2.32%)	6.63 (±4.83%)
			735	1,847 (±0.446%)	250 (±0.682%)					
			775	1,536 (±0.451%)	203 (±0.693%)					
$CuBF_4$	K_{a1} (M^{-1})	K_{a2} (M^{-1})	λ (nm)	ϵ_{HG} (M^{-1})	ϵ_{H_2G} (M^{-1})	K_{a1} (M^{-1})	K_{a2} (M^{-1})	Trial	δ_{HG} (ppm)	δ_{H_2G} (ppm)
	339236 (±2.53%)	606232 (±2.53%)	550	1,610 (±1.38%)	225 (±21.3%)	181956 (±37.3%)	45750 (±43.0%)	1	0.446 (±2.00%)	1.59 (±19.6%)
			575	1,655 (±1.35%)	240 (±20.1%)			2	0.433 (±2.15%)	1.74 (±18.4%)
			650	1,510 (±1.187%)	271 (±16.4%)			3	0.457 (±1.87%)	1.57 (±19.6%)
			735	1,202 (±0.912%)	278 (±14.2%)					
			775	1,014 (±1.05%)	235 (±14.9%)					

Table A.3: Uncoupled full 2:1 host:guest model fits for UV-Vis and ^{1}H NMR. Initial guesses: K_{a1} = 1 M^{-1} , K_{a2} = 10000 M^{-1}, ϵ_{HG} = 10000 M^{-1}, ϵ_{H2G} = 10000 M^{-1}, δ_{HG} = 1 ppm, and δ_{H2G} = 1 ppm.

	Uncoupled UV-Vis					Uncoupled ^{1}H NMR				
$CuPF_6$	K_{a1} (M^{-1})	K_{a2} (M^{-1})	λ (nm)	ϵ_{HG} (M^{-1})	ϵ_{H_2G} (M^{-1})	K_{a1} (M^{-1})	K_{a2} (M^{-1})	Trial	δ_{HG} (ppm)	δ_{H_2G} (ppm)
	0.00134 (±5.22%)	12,524,038 (±1.22%)	550	1,260,905 (±1.68%)	1,404,831 (±7.81%)	138,009 (±52.9%)	41,460 (±53.5%)	1	0.455 (±1.84%)	1.97 (±15.3%)
			575	1,262,650 (±1.52%)	1,436,732 (±5.52%)			2	0.423 (±1.93%)	2.02 (±14.4%)
			650	1,256,888 (±1.11%)	1,337,134 (±3.91%)			3	0.444 (±1.84%)	2.02 (±14.7%)
			735	1,245,849 (±0.679%)	1,143,821 (±7.73%)					
			775	1,233,771 (±0.688%)	929,314 (±7.68%)					
$CuBF_4$	K_{a1} (M^{-1})	K_{a2} (M^{-1})	λ (nm)	ϵ_{HG} (M^{-1})	ϵ_{H_2G} (M^{-1})	K_{a1} (M^{-1})	K_{a2} (M^{-1})	Trial	δ_{HG} (ppm)	δ_{H_2G} (ppm)
	0.00124 (±13,874%)	12,524,052 (±2.58%)	550	1,261,335 (±2.58%)	1,414,472 (±2.58%)	112,303 (±62.5%)	35,347 (±58.7%)	1	0.404 (±2.29%)	2.57 (±13.7%)
			575	1,262,532 (±2.58%)	1,436,180 (±2.58%)			2	0.390 (±2.47%)	2.74 (±13.2%)
			650	1,256,062 (±2.58%)	1,322,797 (±2.58%)			3	0.418 (±2.12%)	2.54 (±13.7%)
			735	1,245,888 (±2.58%)	1,144,531 (±2.58%)					
			775	1,234,066 (±2.58%)	933,149 (±2.58%)					

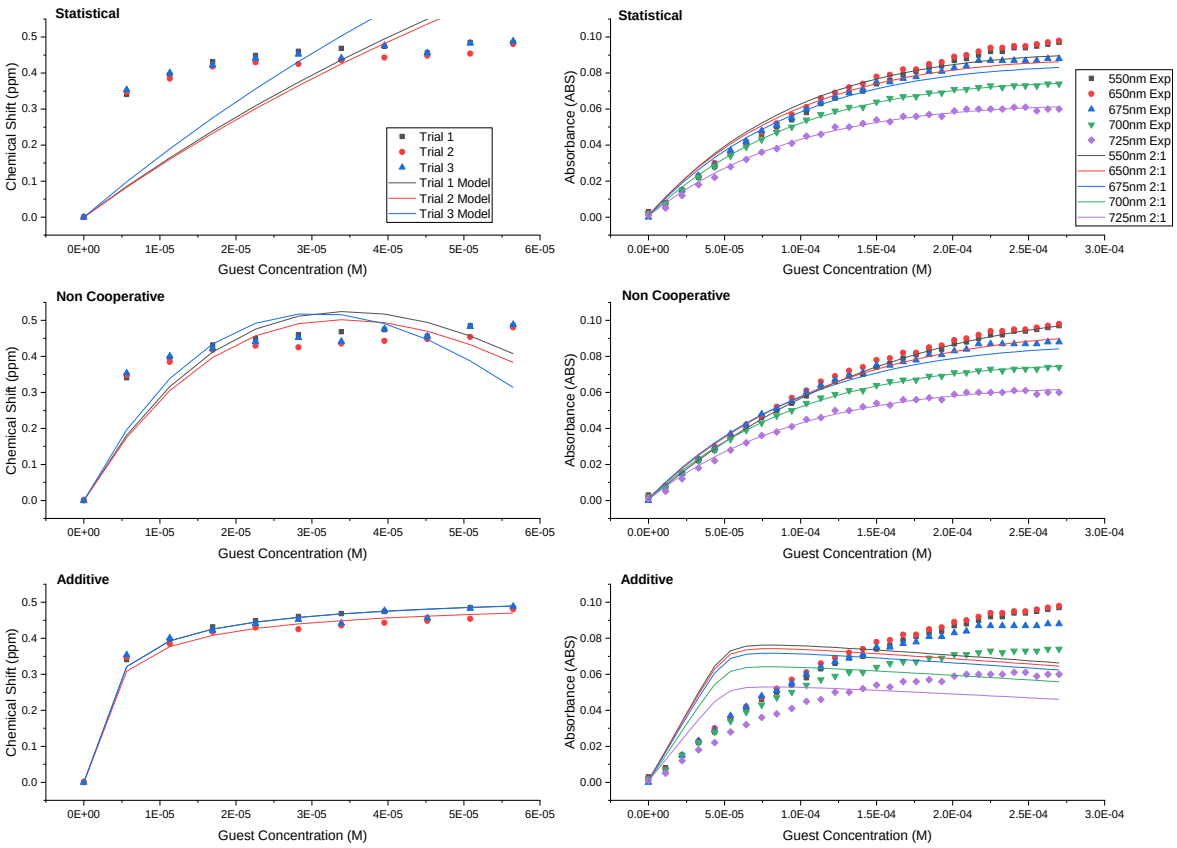

Figure A.4: Titrations of Cu(I)PF_6 into ATF fit to the 2:1 host:guest binding model variations for coupled UV-Vis and NMR models. (Top) Statistical, (Middle) Non-Cooperative, and (Bottom) Additive.

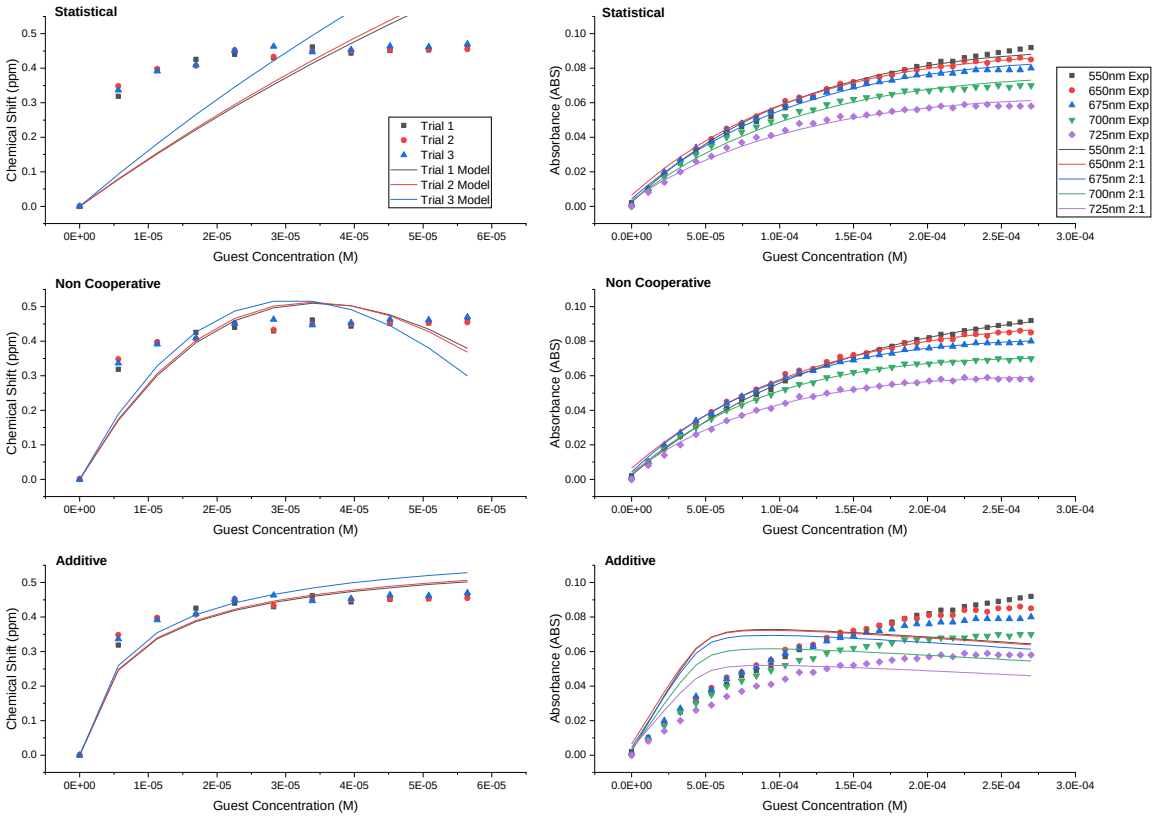

Figure A.5: Titrations of Cu(I)BF_4 into ATF fit to the 2:1 host:guest binding model variations for coupled UV-Vis and NMR models. (Top) Statistical, (Middle) Non-Cooperative, and (Bottom) Additive.